Development of guggulsterone-releasing microspheres for directing the differentiation of human induced pluripotent stem cells into neural phenotypes

by

Andrew Agbay
B.Sc., University of Victoria, 2014

A Thesis Submitted in Partial Fulfillment
of the Requirements for the Degree of

MASTER OF SCIENCE

in the Division of Medical Sciences
(Neuroscience)

Supervisory Committee

Development of guggulsterone-releasing microspheres for directing the differentiation of human induced pluripotent stem cells into neural phenotypes

by

Andrew Agbay
B.Sc., University of Victoria, 2014

Supervisory Committee

Dr. Stephanie Willerth (Division of Medical Sciences)
Supervisor

Dr. Leigh Anne Swayne (Division of Medical Sciences)
Departmental Member

Dr. Brian Christie (Division of Medical Sciences)
Departmental Member

Abstract

In the case of Parkinson's disease, a common neurodegenerative disorder, the loss of motor function results from the selective degeneration of dopaminergic neurons (DNs) in the brain. Current treatments focus on pharmacological approaches that lose effectiveness over time and produce unwanted side effects. A more complete concept of rehabilitation to improve on current treatments requires the production of DNs to replace those that have been lost. Although pluripotent stem cells (PSCs) are a promising candidate for the source of these replacement neurons, current protocols for the terminal differentiation of DNs require a complicated cocktail of factors. Recently, a naturally occurring steroid called guggulsterone has been shown to be an effective terminal differentiator of DNs and can simplify the method for the production of such neurons. I therefore investigated the potential of long-term guggulsterone release from drug delivery particles in order to provide a proof of concept for producing DNs in a more economical and effective way. Throughout my study I was able to successfully encapsulate guggulsterone in Poly-ε-caprolactone (PCL)-based microspheres and I showed that the drug was capable of being released over 44 days *in vitro*. These guggulsterone-releasing microspheres were also successfully incorporated in human induced pluripotent stem cell (hiPSC)-derived neural aggregates (NAs), providing the foundation to continue investigating their effectiveness in producing functional and mature DNs. Together, these data suggest that guggulsterone delivery from microspheres may be a promising approach for improving the production of implantable DNs from hiPSCs.

Table of Contents

Supervisory Committee ii
Abstract iii
Table of Contents iv
List of Figures v
List of Abbreviations vii
Acknowledgments i
Dedication ii
Chapter 1 - Introduction 1
1.1 Parkinson's Disease 1
1.2. PSCs and their properties 4
1.3. Production of DNs from PSCs 6
1.4. Microspheres 16
1.5. Objectives and methodology 18
Chapter 2 - Materials and Methods 20
2.1. Materials 20
2.2. Preparation of single emulsion microspheres 21
2.3. Characterization of microspheres 21
2.3.1. Characterization of surface morphology and particle size analysis 21
2.3.2. Drug encapsulation efficiency 22
2.4. *In vitro* guggulsterone release study 23
2.5. Pluripotent stem cell culture 24
2.5.1. Stem cell maintenance 24
2.5.2. Stem cell aggregate formation 24
2.6. Analysis 25
2.6.1. Immunocytochemistry 25
2.6.2. Neurite morphology 26
2.7. Statistical analysis 26
Chapter 3 - Results 28
3.1. Microsphere characterization 28
3.2. Microsphere incorporation 34
3.3 Immunocytochemistry 36
Chapter 4 - Discussion 50
4.1. Microsphere characterization 50
4.2. Microsphere incorporation and immunocytochemistry 55
4.3 Future directions 60
4.4 Conclusions 62
Bibliography 63

List of Figures

Figure 1. Signalling pathways involved in the maintenance of pluripotency in human stem cells. 7
Figure 2. Pluripotent stem cell differentiation into ectoderm and neural fates. 10
Figure 3. Factors used in recent successful protocols for generating DNs from stem cells. 13
Figure 4. Formation of celluar aggregates from pluripotent stem cells. 18
Figure 5. SEM images showing size distribution and morphology of PCL-based guggulsterone-encapsulated microspheres. 30
Figure 6. Probability density of microsphere diameters produced from the histogram of measured microsphere diameters. 31
Figure 7. Guggulsterone remaining inside of PCL-based microspheres during the *in vitro* release study after predetermined time points over 44 days. 32
Figure 8. *In vitro* cumulative guggulsterone release from PCL-based microspheres over 44 days during the release study. 33
Figure 9. Bright field images of neural aggregate formation with Aggrewell plates. 35
Figure 10. Immunocytochemistry images of a neural aggregate containing guggulsterone microspheres after 12 days *in vitro*. 37
Figure 11. Immunocytochemistry images of a positive control neural aggregate after 12 days *in vitro* with soluble guggulsterone added to the media. 37
Figure 12. Immunocytochemistry images of a negative control neural aggregate after 12 days *in vitro*. 38
Figure 13. Immunocytochemistry images of a neural aggregate containing guggulsterone microspheres after 20 days *in vitro*. 39
Figure 14. Immunocytochemistry images of a positive control neural aggregate after 20 days *in vitro* with soluble guggulsterone added to the media. 40
Figure 15. Immunocytochemistry images of a negative control neural aggregate after 20 days *in vitro*. 40
Figure 16. Fluorescence image of a neural aggregate containing guggulsterone microspheres after 12 days *in vitro*. 42
Figure 17. Fluorescence image of a positive control neural aggregate after 12 days *in vitro* with soluble guggulsterone added to the media. 43
Figure 18. Fluorescence image of a negative control neural aggregate after 12 days *in vitro*. 44
Figure 19. Fluorescence image of a neural aggregate containing guggulsterone microspheres after 20 days *in vitro*. 45
Figure 20. Fluorescence image of a positive control neural aggregate after 20 days *in vitro* with soluble guggulsterone added to the media. 46
Figure 21. Fluorescence image of a negative control neural aggregate after 20 days *in vitro*. 47
Figure 22. Quantitative analysis of neural aggregate morphology for neurite length and branching after 12 days *in vitro*. 48

Figure 23. Quantitative analysis of neural aggregate morphology for neurite length and branching after 20 days *in vitro*. 49

List of Abbreviations

ACN – Acetonitrile

BDNF – Brain-derived neurotrophic factor

BMP4 – Bone morphogenic protein 4

CNS – Central nervous system

DAPI – 4',6-diamidino-2-phenylindole

DCM – Dichloromethane

GSK3β – Glycogen synthase kinase 3 beta

hiPSC – Human induced pluripotent stem cell

iPSC – induced pluripotent stem cell

KLF4 – Kruppel-like factor 4

NA – Neural aggregate

NGS – Normal goat serum

NPC – Neural progenitor cell

NSC – Neural stem cell

OCT 4 – octamer-binding transcription factor 4

DN – Dopaminergic neuron

EB – Embryoid body

ESC – Embryonic stem cell

FGF2 – Fibroblast growth factor 2

FGF8 –Fibroblast growth factor 8

GDNF –Glial cell line-derived neurotrophic factor

PBS – Phosphate buffered saline

PCL – Poly-ε-caprolactone

PD – Parkinson's disease

PLA – Polylactic acid

PLGA – Polyglycolic acid

PLO – Poly-L-ornithine

PSC – Pluripotent stem cell

SHH – Sonic hedge hog

SOX2 – SRY-box 2

STAT3 – Signal transducer and activator of transcription 3

TGFβ – Transforming growth factor beta

Acknowledgments

I would like to first thank all my fellow lab members who have helped me with everything and anything during my time in the lab. For your encouragement, support, and friendship. Especially to Meghan and John for guiding me though flow cytometry and immunocytochemistry, Jose for assisting me in organizing and starting my project, Laura for helping with the labour-intensive release studies, and Nima for being such a supportive role model.

My gratitude goes out to members of the Swayne Lab who have always helped me whenever I asked for advice, for the use of their equipment, and for being there to wallow in stress with me. The same goes for my fellow graduate students in the Neuroscience Program. I would also like to thank Aman of the Moffitt Lab for helping me run the HPLC machine in addition to the particle analyzer and the staff at the advanced microscopy facility for their instruction on using their really expensive equipment.

I would like to express my sincere appreciation to Dr. Leigh Anne Swayne and Dr. Brian Christie for their invaluable feedback and advice in producing the work leading to the creation of this thesis. Last but undoubtedly not least, I would like to thank Dr. Stephanie Willerth for her unending guidance, unwavering support, and unmeasurable encouragement throughout my entire time as a lowly undergrad and also as a slightly more respectable graduate student.

Dedication

I dedicate this to my family, friends, and to contact lenses for keeping me focused.

Chapter 1 - Introduction

1.1 Parkinson's Disease

The loss of neurons in the central nervous system (CNS) often leads to detrimental changes in the function of the affected individuals. Diseases and disorders of the CNS that result from this neuronal loss are a significant issue in today's healthcare landscape. For instance, a common debilitating outcome associated with neuronal loss is Parkinson's disease (PD). This disorder occurs at an incidence rate of 11 to 19 per 100,000 person-years (Van Den Eeden et al., 2003) and is the second most common neurodegenerative disorder after Alzheimer's disease (de Lau & Breteler, 2006). The disease was first medically reported and described almost two centuries ago by James Parkinson and although the study of PD has been prominent in the scientific community since then, the pathological understanding of PD is still evolving (Beitz, 2014). At the core of the disease, PD results from the degradation of DNs in the substantia nigra pars compacta of the ventral midbrain (Dauer & Przedborski, 2003; Hegarty, Sullivan, & O'Keeffe, 2013). Dopamine is an important neurotransmitter in the CNS regulating many functions including locomotion, emotion, and cognition (Chinta & Andersen, 2005). Receptors for dopamine are classified into two main subtypes, D_1 and D_2, and are expressed in both post-synaptic and pre-synaptic neurons coupled to G protein transduction systems (Jaber, Robinson, Missale, & Caron, 1996). The DNs located in the midbrain provide the main source of dopamine in mammalian systems and the most prominent group of these neurons is located in the ventral midbrain, containing 90% of

the total DNs in the brain (Chinta & Andersen, 2005). In PD, degeneration of DNs in the substantia nigra located in this area contributes to the pathogenesis of the disease. The surviving neurons develop a characteristic abnormality: aggregates called Lewy bodies consisting of clumps of α-synuclein protein (Gorman, 2008). The cause of neuronal degradation is still under investigation and there is evidence that a multitude of factors including oxidative stress, toxin-inducing cell death, and defects in important complexes such as the mitochondrial complex 1 and the ubiquitin-proteasome system play a role (Gorman, 2008). It is still unclear whether α-synuclein aggregation itself is the cause of PD or just a characteristic marker of the disease (Kalia & Lang, 2016).

During the disease, the depletion of DNs directly results in the deficiency of dopamine released to the basal ganglia, a group of nuclei in the forebrain that coordinates movement (Blandini, Nappi, Tassorelli, & Martignoni, 2000). Specifically, lost inputs of DNs projecting to the caudate and putamen, collectively known as the striatum, affects the outputs of the pathway which controls voluntary movement (Chinta & Andersen, 2005). Such a deficiency produces impairments involving motor control and function in affected individuals. These impairments are manifested in cardinal symptoms including bradykinesia, resting tremors, and rigidity (Postuma et al., 2015). However, in later stages of PD, non-motor symptoms can arise in the development of sleep issues, autonomic dysfunction, and cognitive decline including dementia (Garcia-Ptacek & Kramberger, 2016; Weerkamp et al., 2013). The disease itself is usually not the direct cause of death but impairments in movement caused by PD are a significant contributing factor. Among patients with PD, the leading cause of death is pneumonia, which is likely due to immobility and increased risk of aspiration from PD motor symptoms (Hely et al., 1999).

Although the brain pathology and symptoms of PD have long been established, the definitive molecular mechanisms behind DN loss remain largely unknown.

Since the body is unable to regenerate and replace neurons that are lost due to PD, this disease creates a challenging problem for rehabilitation and treatment (Benowitz & Yin, 2007). The current most accepted practice for the treatment of PD focuses on the strategy of alleviating the deficiency of dopamine with L-DOPA, also known as Levodopa, which is a precursor to dopamine that is able to cross the blood-brain barrier (Fahn, 2015). Although the use of L-DOPA is useful for controlling PD symptoms, side effects of motor fluctuations and dyskinesias along with a decreased patient response to the drug over time limits the effectiveness of the drug (Jankovic & Aguilar, 2008; Miyasaki, 2016). Although pharmacological treatments such as L-DOPA target the deficiency of dopamine to correct some symptoms of PD, these treatments are unable to slow down or combat the progression of the disease and do nothing to repair damaged DNs; as the disease progresses, these treatments become less effective. While L-DOPA remains the most common therapy for PD motor symptoms, these underlying complications and shortcomings demand a more complete, effective, and long-lasting treatment of the disease. As such, cell replacement therapies for PD remain a likely candidate to combat the disease in its entirety. Accordingly, with PD being a perfect target for the replacement of cells to regain function, Lorenz Studer at the Memorial-Sloan Kettering Cancer Center is hoping to lead clinical trials in the next few years to test the implantation of stem cell-derived DNs in patients with PD (Stoker & Barker, 2016).

1.2. PSCs and their properties

PSCs are characterized by pluripotency and immortality: their ability to become any cell-type in the body while being able to continuously self-renew. In fact, evidence of these cells goes back to the 1960s when Canadian scientists James Till and Ernest McCulloch performed transplant experiments with the bone marrow of mice. These experiments lead to the observation of multipotent donor cells which gave rise to multiple types of blood cells (Becker, Mc, & Till, 1963). The first type of PSC discovered were murine embryonic stem cells (ESCs) in 1981 by Evans and Kaufman through the isolation of cells from the inner cell mass of the blastocyst in mice embryos (Evans & Kaufman, 1981). Subsequently, Thomson et al. were the first to isolate human ESCs in 1998, reporting the same properties as murine ESCs (Thomson et al., 1998). Although nuclear transfer has been used since 1997 to reprogram mammalian somatic cells to PSCs (Wilmut, Schnieke, McWhir, Kind, & Campbell, 1997), the discrete set of transcription factors that regulate pluripotency was not confirmed until 2006 when Takahashi et al. generated the first induced pluripotent stem cells (iPSCs) by direct reprogramming of murine fibroblasts into PSCs (Takahashi & Yamanaka, 2006). In this paper, 24 candidate genes that had been identified to potentially affect pluripotency were tested for their ability to induce pluripotency in somatic cells. Successful reprogramming was achieved by viral transduction with a combination of four important factors – octamer-binding transcription factor 4 (OCT4), SRY-box 2 (SOX2), Kruppel-like factor 4 (KLF4), and c-Myc – and these factors were ultimately dubbed Yamanaka factors with the subsequent reprogramming of human fibroblasts in 2007 by the same group (Takahashi et al., 2007). iPSCs, like ESCs, can differentiate into any cell type in the body and can self-renew

indefinitely (Takahashi, et al., 2007). Recently, iPSCs have been shown to have similar genomes and transcriptomes to ESCs, however, the epigenetic memory and methylation of DNA exhibited in iPSCs may influence differentiation compared to ESCs (Kim et al., 2010; Shutova et al., 2016).

There are other sources of stem cells as well. Neural stem cells (NSCs) are present during adulthood and can also provide a source for producing neurons and glia for replacement therapies. NSCs are endogenous multipotent stem cells located in the subventricular zone and subgranular zone of the adult CNS and these existing cells in the brain play a role in continuing adult neurogenesis (Gage & Temple, 2013). Isolation of neural stem cells, *in vitro* proliferation in structures known as neurospheres, and subsequent differentiation into neuronal cells was demonstrated in the early 90's highlighting their regenerative potential (Reynolds & Weiss, 1992). These neural stem cells could differentiate into the three major cell types of the CNS: neurons, astrocytes, and oligodendrocytes. In comparison, iPSCs similarly possess the capability of producing neural cells for cellular replacement, however, in addition to providing an easily harvestable source they also allow the development of patient specific treatments as the neurons produced can be generated from the somatic cells of each patient when reprogrammed into iPSCs. This is important for addressing the issue of immune rejection of transplanted tissue. Certainly, the discovery and development of iPSCs has significant potential for regenerative medicine due to the possibility of creating patient-specific cell tissues reprogrammed from adult cells and the ability to produce PSCs with an easily harvestable source compared to ESCs.

1.3. Production of DNs from PSCs

Stem cells are maintained in a pluripotent state by the presence of specific transcription factors which affect pathways that relate to preventing differentiation, promoting proliferation, and embryonic development (K. G. Chen, Mallon, McKay, & Robey, 2014; Niwa, 2007). In particular, the most heavily studied pathways and cooperative signalling required to maintain pluripotency for human pluripotent stem cells include the fibroblast growth factor (FGF2) pathway, Wnt pathway, Activin/Nodal pathway, and transforming growth factor beta (TGFβ) pathway (Bieberich & Wang, 2013; K. G. Chen, et al., 2014; James, Levine, Besser, & Hemmati-Brivanlou, 2005; Sato et al., 2003; Vallier, Alexander, & Pedersen, 2005; Xiao, Yuan, & Sharkis, 2006; Xu et al., 2005). All the aforementioned signalling pathways summarized in **Figure 1** converge on regulating a number of transcription factors, most importantly, OCT4, SOX2, and Nanog (X. Chen, Vega, & Ng, 2008; Rodda et al., 2005). These transcription factors are involved in an autoregulatory network to enhance their own expression, binding the promoter regions of the other's including their own.

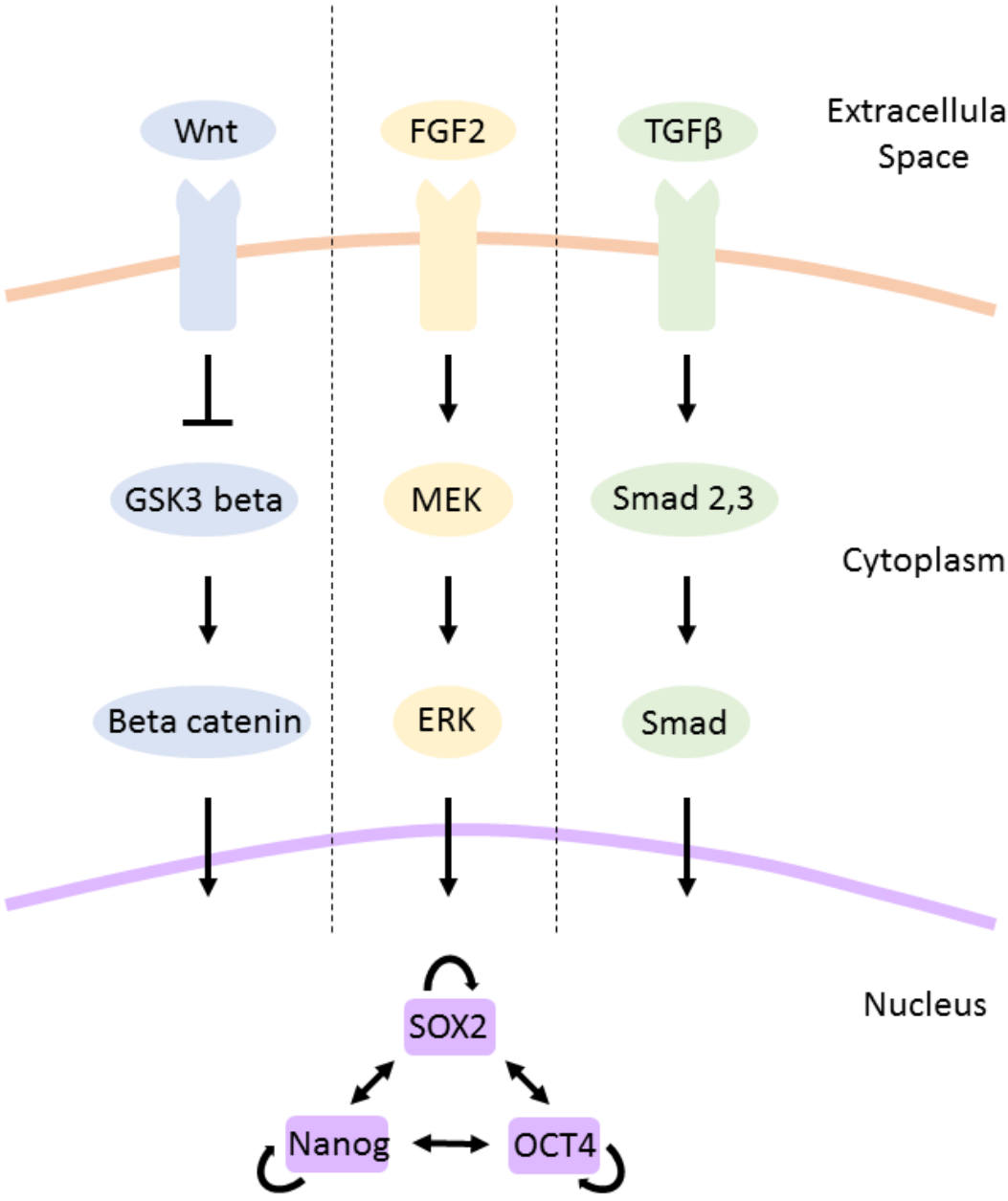

Figure 1. Signalling pathways involved in the maintenance of pluripotency in human stem cells.

Human pluripotent stem cells maintain their pluripotent state through three main pathways: Wnt, TGFβ/Activin/Nodal, and FGF signalling. Translocation of each pathway's products into the nucleus influences the expression of OCT4, Nanog, and

SOX2 that act together to regulate their own promoters and maintain self-renewal and pluripotency. Figure adapted from Bieberich and Wang (Bieberich & Wang, 2013).

Human PSCs can be maintained in a growth medium containing factors that affect the aforementioned pathways. Recently, a feeder-free, serum-free, xeno-free, and chemically defined medium was developed with an essential eight ingredients ($NaHCO_3$, insulin, selenium, transferrin, L-ascorbic acid, FGF2 and TGFβ/Nodal in DMEM/F12) to maintain human pluripotent stem cells *in vitro* (G. Chen et al., 2011).

One method to differentiate PSCs *in vitro* is done by direct treatment of the cells with soluble factors to direct their growth. Another approach uses co-culture with growth of PSCs on a stromal feeder layer to influence growth. These two methods, co-culture on a feeder layer and treatment of soluble factors, can be combined as well. A third approach is to culture PSCs in aggregates called embryoid bodies (EBs) and inducing differentiation by introducing soluble factors (Thomson, et al., 1998). The formation of EBs is one of the oldest methods for differentiation and was even used in the original papers that derived mouse ESCs in 1981 in order to confirm pluripotency (Evans & Kaufman, 1981; Martin, 1981). Although EBs can give rise to heterogenous patterns of differentiated cell types, they are also able to respond to cues that direct embryonic development such as the use of growth factors present in the spatial patterning of the embryo to produce cells of certain types (Murry & Keller, 2008). Similarly, the use of EBs for reliable differentiation of PSCs into specific cell types has been demonstrated previously (Carpenedo et al., 2009; Lee, Lumelsky, Studer, Auerbach, & McKay, 2000; Zhang, Wernig, Duncan, Brustle, & Thomson, 2001). Additionally, it is thought that the 3D structure of the EB allows for a more complete recapitulation of cellular adhesion and

intracellular signalling present in embryonic development (Carpenedo, et al., 2009; Lake, Rathjen, Remiszewski, & Rathjen, 2000). In fact, further advances in the culturing of EBs have produced aggregates, called gastruloids, which exhibit some parallels with embryonic development such as axis formation, germ layer specification, and symmetry breaking (van den Brink et al., 2014).

To induce differentiation of PSCs to a neural lineage, inhibition of the TFGβ, Activin/Nodal, and Wnt pathways is required for ectodermal specification (Murry & Keller, 2008). Additionally, inhibition of bone morphogenic protein 4 (BMP4) prevents ectodermal PSCs from differentiating into skin cells and instead they differentiate into nerve cells (Murry & Keller, 2008; Patthey & Gunhaga, 2014). At this point it is also thought that FGF2 has a role in neuronal differentiation promoting neural specification (Murry & Keller, 2008; Patthey & Gunhaga, 2014; Wilson & Stice, 2006). Neural lineage differentiation from PSCs is summarized in **Figure 2**. Accordingly, during EB formation from PSCs, the inhibition of TFGβ, Activin/Nodal, Wnt, and BMP4 will produce an EB composed of cells with a neural-ectodermal fate destined to become neurons, astrocytes, and oligodendrocytes. Hereafter, such EBs will be referred to as NAs. Media supplemented with factors affecting the aforementioned pathways and produce these NAs are often called neural induction media (NIM).

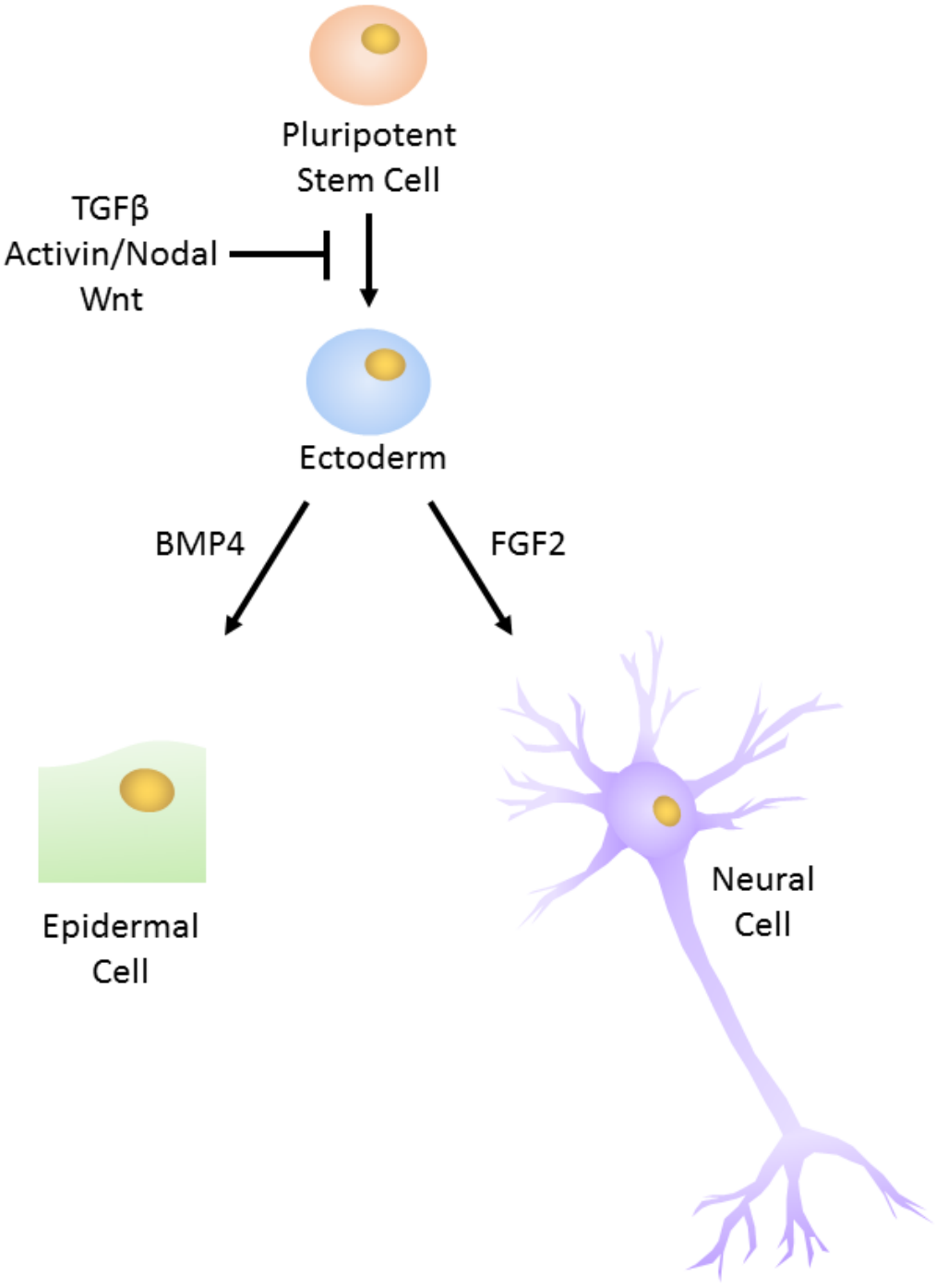

Figure 2. Pluripotent stem cell differentiation into ectoderm and neural fates.

Our understanding of the mechanisms that govern pluripotent stem cell differentiation into specific germ layer identities is still incomplete, however, important signalling pathways involved include Wnt, TGFβ, and Activin/Nodal which play key roles in

maintaining pluripotency of stem cells. In the absence or inhibition of Wnt, TGFβ, and Activin/Nodal, the cells will differentiate to an ectodermal identity. At this point BMP4 signalling promotes epidermal fate while FGF2 promotes neural fate. Figure adapted from Arenas et al., Bieberich and Wang, and Patthey and Gunhaga. (Arenas, Denham, & Villaescusa, 2015; Bieberich & Wang, 2013; Patthey & Gunhaga, 2014).

For DN production, approaches for generating the neuronal subtype focus on the activation of key signalling pathways through treatment with soluble factors. Formation of two important signalling centers occurs during embryonic development: the floor plate which controls ventral specification (Placzek & Briscoe, 2005) and the isthmic organizer which creates the midbrain-hindbrain boundary (Joyner, Liu, & Millet, 2000). This formation step is essential for creation of the ventral midbrain and thus the generation of DNs. The growth factor fibroblast growth factor 8 (FGF8) is sufficient to produce the isthmic organizer and is secreted itself by the organizer to help pattern the anterior-posterior axis (Basson et al., 2008; Chi, Martinez, Wurst, & Martin, 2003; Crossley, Martinez, & Martin, 1996; Fasano, Chambers, Lee, Tomishima, & Studer, 2010; Martinez, Crossley, Cobos, Rubenstein, & Martin, 1999). Similarly, the protein sonic hedgehog (SHH) is expressed by the floor plate to help pattern the ventral-dorsal axis (Briscoe, 2006). In addition, it has also been shown that DNs develop at sites where signals of SHH and FGF8 intersect (Ye, Shimamura, Rubenstein, Hynes, & Rosenthal, 1998).

Accordingly, of all the dopaminergic differentiation factors investigated, treatment with SHH and FGF8 have been the most common with some protocols using additional molecules in conjunction with the two (Arenas, et al., 2015; Friling et al., 2009; Kriks et al., 2011; Lee, et al., 2000; Y. Yan et al., 2005). Some of these protocols

use a small molecule called puromorphamine in place of or in combination with SHH. Purmorphamine is a synthetic molecule that activates the SHH pathway (Briscoe, 2006; El-Akabawy, Medina, Jeffries, Price, & Modo, 2011). Advantages of its use in lieu of SHH includes stability and affordability due to being commercially produced. Lorenz Studer's group, a lab that has worked on cell therapies for PD for over a decade, started with a stromal feeder co-culture for hESC dopaminergic differentiation in 2004 and has adopted the use of SHH and FGF8 in their soluble factor strategy in more recent publications (Chambers et al., 2009; Kriks, et al., 2011; Perrier et al., 2004). In these recent publications, along with others, a more efficient method of producing DNs was discovered by including the use of glycogen synthase kinase 3 beta (GSK3β) inhibitors to help initiate differentiation with additional molecules in a final maturation stage composed of a complex mixture of growth factors and chemicals (including a subset or combination of brain-derived neurotrophic factor (BDNF), glial cell line-derived neurotrophic factor (GDNF), Dibutyryl-cAMP, TGFβ3, DAPT, and ascorbic acid) (Arenas, et al., 2015; Kirkeby et al., 2012; Kriks, et al., 2011). **Figure 3** presents a visual depiction of the common factors used for DN production in these studies. GSK3β inhibitors were used to induce Wnt/β-catenin signalling when it was discovered to be an essential pathway in DN development (Castelo-Branco, Rawal, & Arenas, 2004; Castelo-Branco et al., 2003; Tang et al., 2010). The factors used in the final maturation stage have all been implicated in the differentiation and/or survival of DNs. For example, BDNF and GDNF have been shown to increase survival and arborisation (branching) of DNs in primary neuronal culture (K. D. Beck et al., 1995; Costantini & Isacson, 2000). TGFβ3 can promote survival and protection of several DN populations (Roussa, von Bohlen und

Halbach, & Krieglstein, 2009). DAPT can increase neuron marker expression, enhancing neuronal differentiation from ESCs (Crawford & Roelink, 2007). Finally, ascorbic acid and Dibutyryl-cAMP can increase DN yield from rat mesencephalic precursor cells (Mena, Casarejos, Bonin, Ramos, & Garcia Yebenes, 1995; J. Yan, Studer, & McKay, 2001).

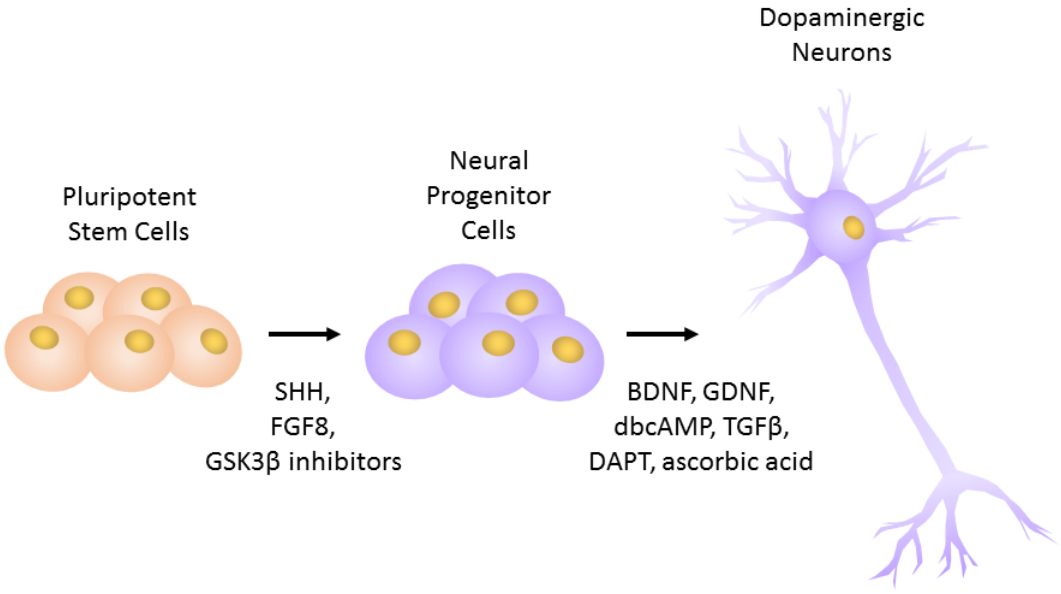

Figure 3. Factors used in recent successful protocols for generating DNs from stem cells. These protocols include a cocktail of factors required in early differentiation and late stage differentiation. For early differentiation, the use of SHH, FGF8, and GSK3β inhibitors was common to specify growth into neural progenitor cells (NPCs). For late stage differentiation, a combination of factors including BDNF, GDNF, dbcAMP, TGFβ3, DAPT, and ascorbic acid was used to produce mature DNs. Figure adapted from Arenas et al. (Arenas, et al., 2015).

Among the most effective protocols for deriving DNs is a direct differentiation method as described by Kriks et al. from the Studer group producing DNs that were

successfully used to engraft into animal models of PD (Kriks, et al., 2011). These implanted DNs survived up to five months, retained DN marker expression, and induced functional recovery in motor-behavioral tests on three host species. This protocol utilizes GSK3β inhibitors in early differentiation along with all previously mentioned enhancing factors in the final differentiation stage. In wake of this study that demonstrated DN survival and function of engrafted cells, Studer's group is now pursuing human clinical trials for the implantation hESC-derived DNs in patients with PD in the next few years.

Recently, others are focused on fine-tuning the complicated dopaminergic differentiation protocols. In 2013, Gonzalez et al. sought to simplify these protocols by screening 1120 biologically active compounds for their effectiveness in terminal dopaminergic differentiation from hESCs. They identified a steroid called guggulsterone as the most effective inducer of dopaminergic differentiation, replacing the use of GSK3β inhibitors and the complex cocktail used in late stage differentiation with a single factor (Gonzalez et al., 2013). The guggulsterone treated cells exhibited the greatest dopmine release and enhanced mature DN marker expression including 97% positive for the marker tyrosine hydroxylase. With the use of this streamlined protocol, Gonzalez et al. were able to generate DNs that secreted three-fold higher dopamine levels *in vitro* than the Kriks et al. study while having typical DN gene and protein expression profiles as well (Gonzalez, et al., 2013; Kriks, et al., 2011).

Guggulsterone is a naturally occurring steroid found in the gum resin of the guggul tree *Commiphora wightii* and has been used in traditional medicine for centuries to treat a myriad of disorders, some of which include obesity, intestinal worms, and liver disorders (Shishodia, Azu, Rosenzweig, & Jackson, 2016; Yamada & Sugimoto, 2016).

Current research investigates the potential of guggulsterone to regulate cholesterol levels as a farnesoid X receptor antagonist (Yamada & Sugimoto, 2016), suppress pro-inflammatory factors in neuroinflammation (Huang et al., 2016), and effect gene expression of some transcription factors involved with tumorigenesis as an anti-cancer drug (Shishodia, et al., 2016).

To further examine the effectiveness of guggulsterone in DN production, Robinson et al. demonstrated that guggulsterone could also promote high levels of DN differentiation from hiPSCs using both an NA and a direct differentiation method. In addition to confirming the efficacy of guggulsterone on hiPSCs to produce DNs with terminal treatment over 38 days, Robinson et al. found that the NA method was superior to direct differentiation with increased neurite length and branching (Robinson et al., 2015). Although differentiation from cellular aggregates is a common approach, it has limitations in producing a homogenous population of cells with the addition of soluble factors in cell culture medium to differentiate a 3D collection of cells (Bratt-Leal, Carpenedo, & McDevitt, 2009; Carpenedo, et al., 2009). During embryonic development, morphogens are secreted in a specific spatial and temporal manner by the cells inside the embryo whereas soluble factors present in culture medium are added externally to the aggregate which poorly replicates this natural process (Brennan et al., 2001; Corson, Yamanaka, Lai, & Rossant, 2003; Niederreither, Vermot, Schuhbaur, Chambon, & Dolle, 2000). In addition, there has been evidence of mass transfer limitations (Van Winkle, Gates, & Kallos, 2012) and production of structural barriers that restrict diffusive transport within cellular aggregates (Sachlos & Auguste, 2008). Therefore, the use of biomaterial particles, namely microspheres, to control cellular aggregate differentiation

has been investigated to address these problems (Bratt-Leal, et al., 2009; Bratt-Leal, Carpenedo, Ungrin, Zandstra, & McDevitt, 2011; Bratt-Leal, Nguyen, Hammersmith, Singh, & McDevitt, 2013; Carpenedo, et al., 2009; Carpenedo, Seaman, & McDevitt, 2010; Lim et al., 2011; Wang, Yu, Baker, Murphy, & McDevitt, 2016).

1.4. Microspheres

Microspheres are micro-scale particles often made from biodegradable polymers that can be used as drug delivery vehicles (Varde & Pack, 2004). Drugs, including small molecules such as guggulsterone or proteins such as GDNF, can be encapsulated inside of microspheres and be subsequently released over an extended period of time associated with the degradation of the polymer. Selecting specific polymers allow microspheres to be biodegradable and biocompatible in addition to providing controlled drug release (Yang, Chung, & Ng, 2001). In addition, by altering particle size, density, and polymer used during the fabrication process, one can influence the release rate of the encapsulated drug (Coccoli et al., 2008).

Many types of biodegradable polymers such as polylactic acid (PLA), polyglycolic acid (PLGA), and PCL have been utilized in previous microsphere studies due to their biocompatibility in biological systems (Sinha, Bansal, Kaushik, Kumria, & Trehan, 2004). Among them, interest in the use of PCL has been renewed due to its high permeability for small molecules, long-term degradation up to one year, low cost, and inability to produce acidic environments during hydrolysis degradation as compared to PLA and PLGA (Sinha, et al., 2004; Woodruff & Hutmacher, 2010). For creating a drug

delivery system with the aims of reducing cost and allowing for long-term drug release, PCL is a promising candidate.

Microspheres have been previously incorporated into both hiPSC and hESC EBs to investigate their ability to provide controlled drug release for the differentiation of cells throughout the entire cellular aggregate (Bratt-Leal, et al., 2011; Bratt-Leal, et al., 2013; Gomez et al., 2015; Lim, et al., 2011; Qutachi, Shakesheff, & Buttery, 2013). A depiction of such microsphere incorporation inside of cellular aggregates is depicted in **Figure 4**. In addition, other molecule-coated microparticles made from a variety of materials have been incorporated within ESC EBs as well (Bratt-Leal, et al., 2013; Wang, et al., 2016). These studies report successful incorporation of particles inside EBs without deleterious effects on cell viability as well as possible effects of different materials on differentiation (Bratt-Leal, et al., 2011) and effectiveness of microsphere drug delivery compared to soluble factor treatment in the media (Ferreira et al., 2008). In addition, these studies found that decreasing particle diameter (down to 1 μm) increased particle incorporation in EBs and increasing the amount of particles in EBs affected the aggregates ability to stay intact (Carpenedo, et al., 2010; Gomez, et al., 2015). Similarly, the use of microspheres to deliver guggulsterone could be a beneficial strategy in optimizing the differentiation of NAs into DNs.

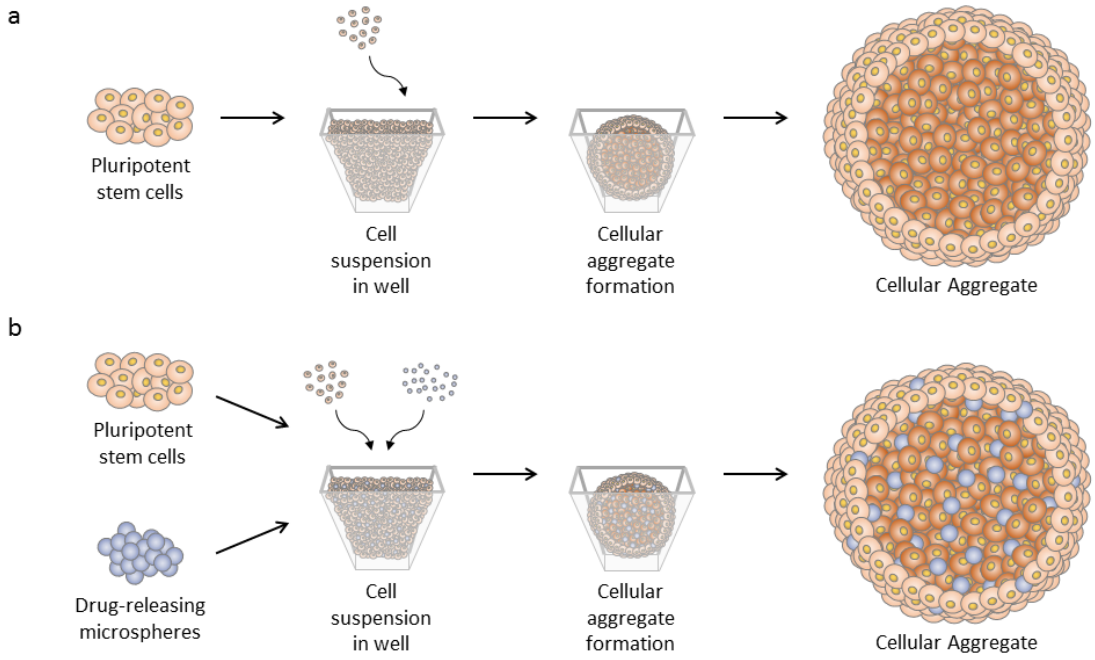

Figure 4. Formation of celluar aggregates from pluripotent stem cells.
(a) A cell suspension of pluripotent stem cells is centrifuged into aggregate-forming microwells. (b) A mixture of pluripotent stem cells and microspheres is centrifuged into aggregate-forming microwells. Aggregates are referred to as EBs if they contain the ability to differentiate into all three germ layers and as NAs if they are specified to a neural fate. For example, NA formation is complete after 5 days of growth in NIM. Aggregates are then harvested and plated on cell culture-treated surfaces for subsequent differentiation and growth.

1.5. Objectives and methodology

Previous studies have looked at delivering small molecules for differentiation by the incorporation of microspheres inside of NAs (Gomez, et al., 2015) and the effectiveness of guggulsterone in the differentiation of DNs from NAs (Robinson, et al., 2015). Although guggulsterone has the potential to make the DN differentiation protocol

cheaper, simpler, and more effective, there has been little research on the subject. To date, there has been no published research on the controlled release of guggulsterone from biomaterial scaffolds including microspheres. The use of a biodegradable drug delivery system for the release of guggulsterone could decrease the labour of daily media changes, reduce the amount of drug needed to differentiate PSCs through delivery within cellular aggregates, and provide a way to extend terminal differentiation *in vivo*. This study investigates a possible method of guggulsterone delivery for long-term release in the differentiation of hiPSCs.

Due to the promising potential of guggulsterone to be a terminal dopaminergic differentiator, the first aim of this study was to be able to fabricate microspheres that could deliver guggulsterone for at least 38 days, the time course of treatment used by Robinson et al. (Robinson, et al., 2015). A 44 day release study was chosen to cover the aforementioned time course while going beyond to one and a half months to observe release kinetics further than the stopping time points in previous studies (Agbay, Mohtaram, & Willerth, 2014; Gomez, et al., 2015). The second aim of this study was to investigate the compatibility of the microspheres with hiPSCs by incorporating them into NAs at the easiest time point during aggregate formation. To properly recapitulate previous guggulsterone differentiation protocols, incorporation with later stage (day 19) NPCs after treatment with SHH and FGF8 must be done, however, this study acts as a stepping stone to that goal. Cursory effects on influencing differentiation and growth were also examined to direct future studies.

Chapter 2 - Materials and Methods

2.1. Materials

Poly (Ɛ-caprolactone) (PCL) (Mn ~ 45,000), polyvinyl alcohol (PVA) (M w ~ 13,000–23,000, 87–89% hydrolyzed), (E)-guggulsterone (≥95% HPLC, powder), laminin from Engelbreth-Holm-Swarm murine sarcoma basement membrane, poly-L-ornithine (PLO) 0.01% solution, Normal goat serum (NGS), and Triton X-100 were purchased from Sigma-Aldrich (St. Louis, MO, USA). Dichloromethane (DCM) was purchased from Fisher Scientific (Ottawa, ON, Canada). Goat anti-mouse IgG (H+L) highly cross-adsorbed secondary antibody, Alexa Fluor® 488 and 4,6-diamidino- 2-phenylindole, dihydrochloride (DAPI) nucleic acid stain was purchased from Thermo Fisher Scientific (Waltham, MA, USA). Anhydrous ethyl alcohol was purchased from Commercial Alcohols (Brampton, ON, Canada). Acetonitrile (ACN) HPLC 190 was purchased from Caledon Laboratory Chemicals (Georgetown, ON, Canada). Phosphate buffer solution (PBS) was purchased from Invitrogen (Burlington, ON, Canada). TeSR™-E8™ Kits for hESC/hiPSC Maintenance, Vitronectin XF™ Kits, STEMdiff™ Neural Induction Medium, AggreWell™800 plates, anti-beta-tubulin III mouse monoclonal [clone AA10] IgG2a antibody, and ReLeSR™ were purchased from STEMCELL Technologies (Vancouver, BC, Canada). Undifferentiated hiPSCs (iPS(Foreskin)-1, Lot 1-DL-01) were purchased from WiCell (Madison, WI, USA).

2.2. Preparation of single emulsion microspheres

Microspheres were fabricated using an oil-in- water (o/w) emulsion followed by the evaporation of the organic solvent as previously described (Gomez, et al., 2015). For the water phase, 2% PVA solution was made by dissolving PVA in de-ionized water for 1 hour at 85°C while mixing at a speed of 850 rpm on a Corning PC-420D magnetic mixer. 100 mL of 0.3% (w/v) PVA solution was made by diluting 2% PVA with de-ionized water and held at 35°C. 500 mg of PCL was dissolved in 3 mL of DCM on a magnetic mixer for 15 minutes at 900 rpm to make the oil phase. When making guggulsterone-encapsulated microspheres, 0.3 mg of the drug (dissolved in 100% ethanol) was added to the oil phase to make microspheres at a concentration of 0.6 μg/mg (w/w, guggulsterone/PCL) microspheres. After removing from the magnetic mixer, 3 mL of 2% PVA were slowly added to the oil solution to prevent disruption of the boundary layer. An emulsion of the solution (w/o) was then produced by vortex mixing (Fisher Scientific) at 3000 rpm for 15 seconds. This (w/o) emulsion was immediately added to the 0.5% PVA water phase and held at 35°C at a mixing speed of 500 rpm for 4 hours to achieve evaporation of the organic solvent. After mixing, the microspheres were isolated by centrifugation at 4000 rpm (Eppendorf 5810R) and washed with de-ionized water. For long-term storage, the microspheres were lyophilized for 24 hours and stored at -20°C.

2.3. Characterization of microspheres

2.3.1. Characterization of surface morphology and particle size analysis

Morphological characterization was performed using a Hitachi S-4800 FE scanning electron microscopy (SEM) machine to image the microspheres after fabrication as done previously (Agbay, et al., 2014; Gomez, et al., 2015). Lyophilized microspheres were transferred to loading stubs by ethanol suspension and evaporation, then coated with gold-palladium using an Anatech Hummer VI sputter coater to enhance surface conductivity. Images were captured using an accelerated voltage of 1.0 at working distances of 8.2 mm and 7.8 mm. The average diameter of the microspheres was determined in two ways: the first by using the ImageJ image processing program to conduct manual diameter measurements on SEM microsphere images and the second by the use of a ZetaPALS zeta potential/particle size analyzer (Brookhaven Instrument Corp.).

2.3.2. Drug encapsulation efficiency

The amount of guggulsterone encapsulated per unit weight of microspheres was determined by extraction of the drug from the fabricated microspheres. A measured amount of lyophilized microspheres was placed in a 1.5 mL propylene microtube and 200 uL of ACN were added to each sample. The samples were vortexed at 3000 rpm for 30 seconds, vortexed for 5 minutes at 350 rpm (Eppendorf® MixMate®), and mixed with a micropipette for 10 seconds. These mixing steps were repeated twice to dissolve the PCL. Next, 1000 uL of additional ACN was added to the samples and mixed by micropipette for 10 seconds then vortexed at 3000 rpm for 30 seconds. The solution was then centrifuged at 22°C at 13000 rpm for 5 min using an Eppendorf 5424 Microcentrifuge. 1000 uL of the supernatant was transferred to a microtube and diluted as necessary for

running on a high performance liquid chromatography-mass spectrometry (HPLC-MS) machine. The concentration of the drug in the sample was determined by HPLC-MS (Ultimate 3000 MSQ, Thermo Scientific with Chromeleon^{TM} software) and run against a guggulsterone standard composed of five dilutions of a stock solution composed of guggulsterone dissolved in ACN. Analysis was done on a C18 column (Phenomenex Luna 5u C18) using a constant eluent mobile phase composition of 80% ACN and 20% water with 0.1% trifluoroacetic acid while detecting at a characteristic absorption wavelength of 255 nm in the ultraviolet-visible spectrum based on the parameters described by Ahkade et al. (Akhade, Agrawal, & Laddha, 2013). The sample injection volume was set at 50 µL and flow rate was set at 1.5 mL/min. To calculate encapsulation efficiency, a comparison of the actual encapsulated guggulsertone ($G_{encapsulated}$) to the amount of guggulsterone originally added ($G_{theoretical}$) was made according to Eq. (1).

$$\text{Encapsulation efficiency} = (G_{encapsulated}/G_{theoretical}) \times 100\% \quad (1)$$

2.4. *In vitro* guggulsterone release study

In vitro release studies were carried out in triplicate. 10 mg of microspheres were suspended in 1 mL of PBS in a microtube. The tubes were then loaded onto a Sarstedt Sarmix mr-1 tube rotator and incubated at 37°C. The PBS supernatant for each tube was replaced every 2 days while tubes were removed and collected from the rotator at predetermined time points: day 2, 4, 8, 12, 16, 20, 24, 28, 36, and 44. For the collected tubes, PBS supernatant was removed and microspheres were washed with deionized

water, lyophilized, and weighed. The remaining guggulsterone concentration inside the microspheres was determined as previously described by dissolving microspheres with DCM, extraction of the drug/precipitation of PCL with 100% ethanol, and having the absorbance read at 255 nm on a Tecan Infinite® M200Pro plate reader (Gomez, et al., 2015). The amount of guggulsterone released was calculated by subtracting the guggulsterone remaining in the microspheres from the theoretical guggulsterone present in each amount of microspheres at day 0.

2.5. Pluripotent stem cell culture

2.5.1. Stem cell maintenance

hiPSCs were maintained in an undifferentiated state on 6-well plates coated with Vitronectin XF™ using TeSR™-E8™ media as previously described (Robinson, et al., 2015). Media was changed daily. For passaging, ReLeSR™ was used to select and remove undifferentiated hiPSCs from the wells. Cells were passaged at a ratio of 1:6 and plated on fresh Vitronectin XF™ coated plates.

2.5.2. Stem cell aggregate formation

ReLeSR™ was used to select and remove undifferentiated hiPSCs from the wells. Uniform hiPSC aggregates were formed by adding a single cell suspension in STEMdiff™ Neural Induction Medium of $1x10^6$ hiPSCs to wells in AggreWell™ 800 plates and centrifuged for 5 min at 100×g to deposit the cells at the bottom of each microwell. Before incorporation with the cells, microspheres were sterilized by low power air-plasma treatment (Harrick PDC-32G) for 30 seconds as described previously (Gomez, et al., 2015). When forming microsphere-incorporated hiPSC aggregates, 0.5

mg of microspheres suspended in STEMdiff™ Neural Induction Medium were added to each AggreWell™ 800 well for a total of 2 mL of media in each well and centrifuged for 5 min at 100×g. The aggregates in the AggreWell™ 800 plates were maintained in 2 mL of STEMdiff™ Neural Induction Medium with daily media changes for 5 days. On day 5, aggregates were harvested for immunocytochemistry or transferred to PLO/laminin-coated 24-well plates at a single aggregate per well for the remaining duration of the cell study (until day 12 or day 20). Positive control treatments contained aggregates without microspheres and guggulsterone in the media at a concentration of 2.5 μM. Negative control treatments contained aggregates without microspheres and media without soluble drug added.

2.6. Analysis

2.6.1. Immunocytochemistry

After growth to 12 or 20 days, cell aggregates were washed with PBS and then fixed with 10% formalin for 1 hour. Next, the cells were permeabilized in 0.1% Triton X-100 in PBS for 45 minutes at 4°C then blocked with 5% NGS in PBS for 2 hours at 4°C. Primary antibody anti-beta-tubulin III diluted 1:1000 in 5% NGS was added and incubated overnight at 4°C. The aggregates were then washed with PBS three times and secondary antibody Alexa Fluor® 488 goat anti-mouse IgG diluted 1:500 in 5% NGS was added and incubated for 4 hours at 25°C. Following incubation, the cells were washed three times and counterstained with DAPI, a nucleic acid stain, at a concentration of 300 nM incubated for 3 minutes and then rinsed with PBS. Cells were then visualized with a Leica DMI3000 B microscope using an XCite Series 120Q fluorescent light source and

QImaging RETIGA 2000R camera at 100X magnification. Images were captured using QCapture Software 2.9.12.

2.6.2. Neurite morphology

Immunostained neural aggregates were imaged with an IncuCyte® ZOOM automatic live-cell imaging system (Essen BioScience, Ann Arbor, MI) at 10X magnification. Quantification of the morphological metrics of neurite length and branch points was done by IncuCyte® ZOOM Software (2016A). Using the NeuroTrack™ software module, day 12 and day 20 green channel fluorescence (anti-beta-tubulin III positive) images were analyzed by masking total neurite coverage and calculating average length and branch points with the same processing definition. Neural aggregate area analysis was done for day 12 images by a NeuroTrack™ software processing definition whereas a Basic Analyzer processing definition (used for confluence masking) analyzed day 20 images. Metrics were calculated per single aggregate with two aggregates per treatment group for all negative and positive control time points and one aggregate per treatment group for microsphere-incorporated time points. Composite neural aggregate images were created using the Magic Montage plugin for the ImageJ image-processing program.

2.7. Statistical analysis

Results are reported as mean values ± standard deviation of the mean. Statistical analysis was performed with the Minitab® 17.3.1 statistics software applying standard t-test analysis on neurite morphology metrics with a 95% confidence level where

significance is considered for $p < 0.05$.

Chapter 3 - Results

3.1. Microsphere characterization

Guggulsterone-containing microspheres were fabricated by a single emulsion technique and were imaged with an SEM to determine their morphology and size distribution (**Fig. 5**). The microspheres displayed a spherical shape with smooth surfaces while their diameters were not uniform. Through hand-measuring microsphere diameters with SEM images, the average diameter was calculated to be 6.14 ± 9.09 μm while the median was 3.28 μm (**Fig. 6**). Similarly, measuring microsphere diameters with a particle-sizer yielded an average microsphere diameter of 14.8 ± 5.9 μm which, although resides within the standard deviation of the hand-measured average, is more than twice the average diameter calculated from the SEM images. The encapsulation efficiency of guggulsterone inside of the microspheres was 42.4 ± 3.5 % of the total guggulsterone added during the fabrication process. Release kinetics of the drug from the microspheres was observed inversely by determining leftover drug inside the microspheres over a range of sample days ending on day 44 (**Fig. 7**). The slope of the graph exhibits a calculated average release of 37 ng of drug released per day from 10 mg of microspheres. Taking into consideration the theoretical total amount of drug initially in each sample (~2.5 μg in 10 mg of microspheres) on day 0, a cumulative release profile of the drug from the microspheres was calculated (**Fig. 8**). Percentages of the drug that were assumed to be released for each sample day was calculated by comparing drug amounts leftover and initial amounts of the drug inside the microspheres. The cumulative release graph

displays the addition of these percentage amounts up to day 44. On the final day of release studies, the microspheres released ~60% of the drug theoretically encapsulated.

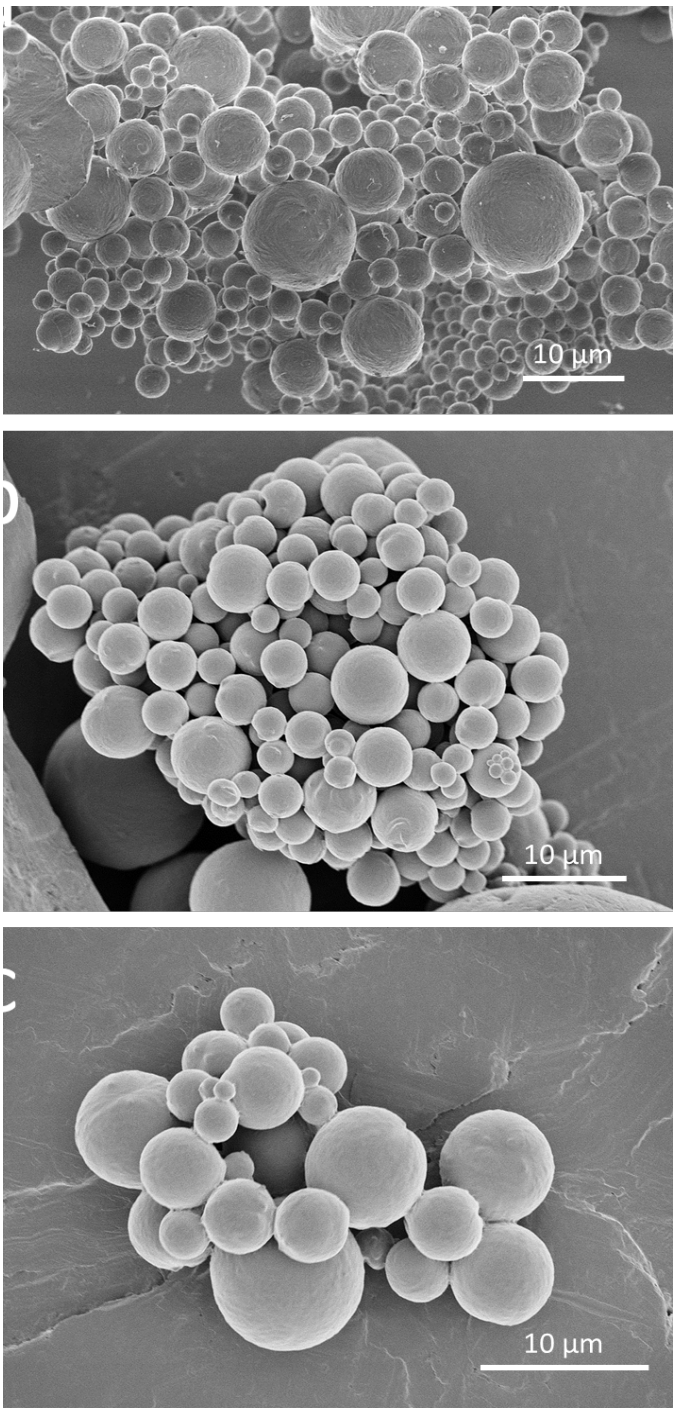

Figure 5. SEM images showing size distribution and morphology of PCL-based guggulsterone-encapsulated microspheres.

Images taken at (a) X1800, (b), X2200, and (c) X3000 magnification show spherical structure, surface morphology, and size variety. An accelerating voltage of 1.0 kV and working distances of 8.2 mm and 7.8 mm were used to capture the images.

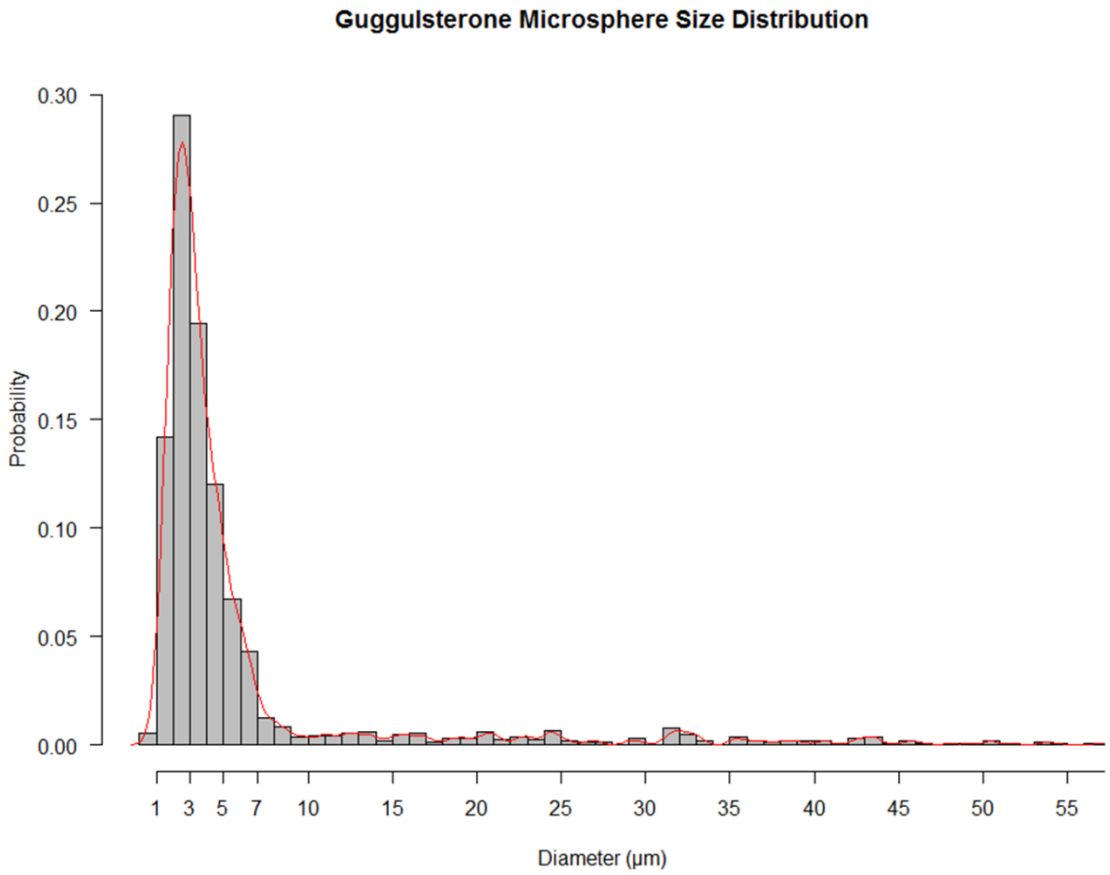

Figure 6. Probability density of microsphere diameters produced from the histogram of measured microsphere diameters.

The median was calculated to be 3.28 µm and average diameter was 6.14 ± 9.09 µm with a sample size of n=1666. Measurements were taken with ImageJ processing software and a kernal density curve was fitted to the probability density plot using the R statistical programming language.

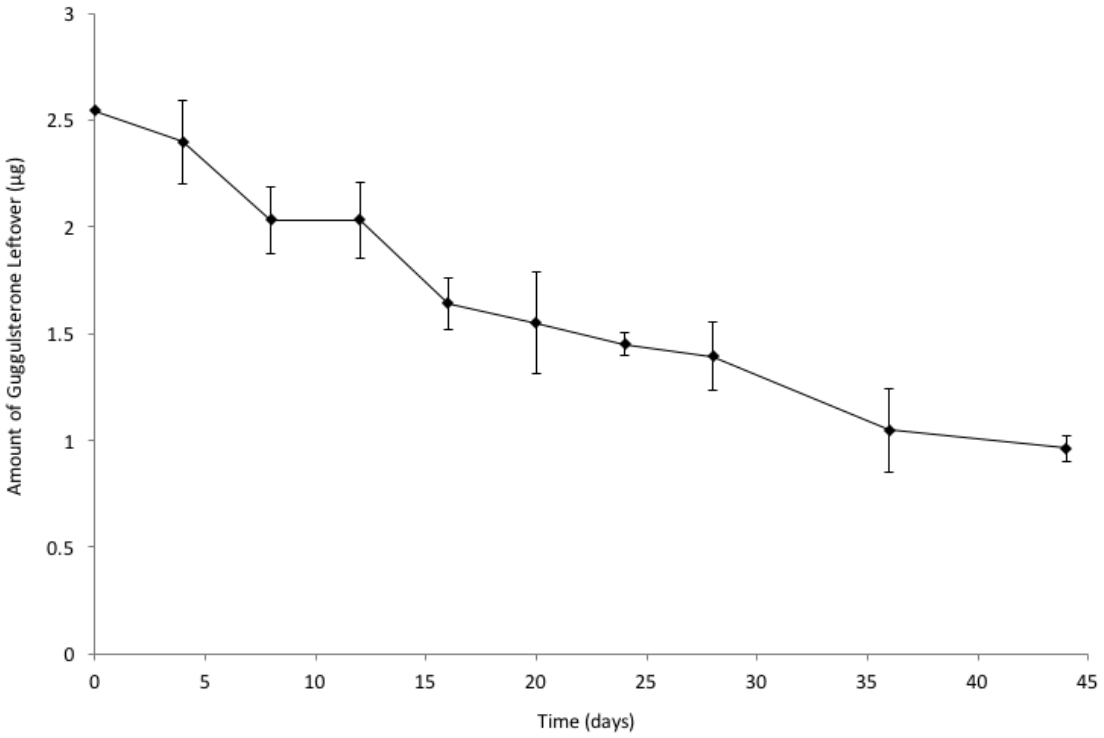

Figure 7. Guggulsterone remaining inside of PCL-based microspheres during the *in vitro* release study after predetermined time points over 44 days.

Data points shown are guggulsterone amounts in µg for each sample vial (~10 mg of microspheres). Standard deviations are shown with a sample size n=3.

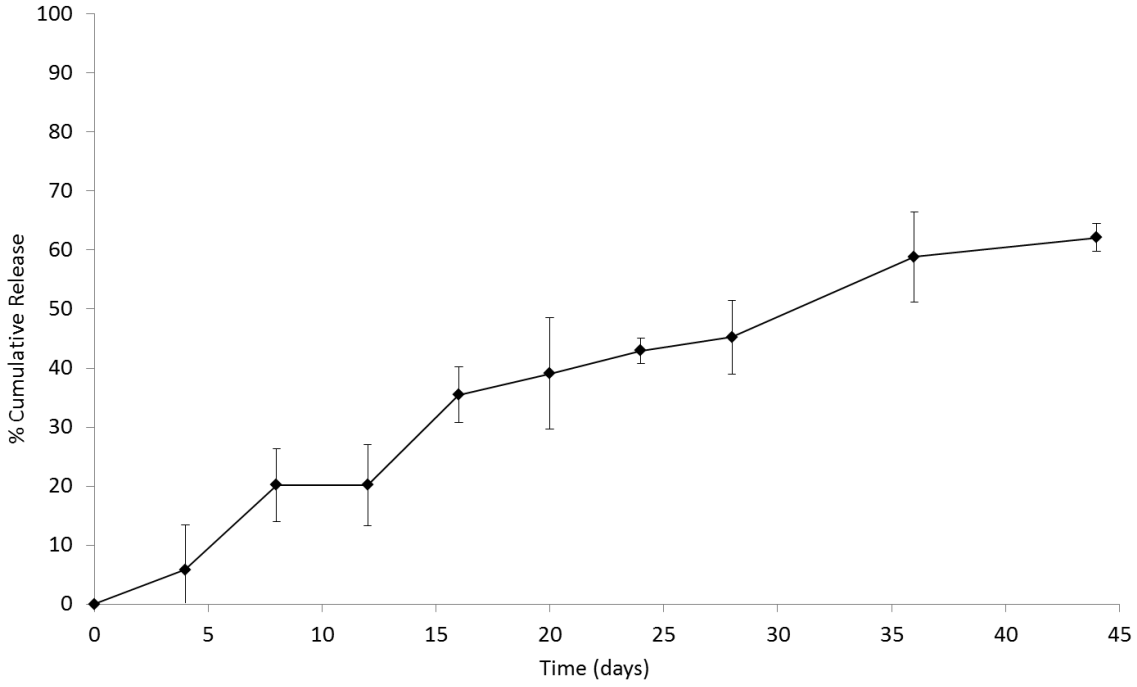

Figure 8. ***In vitro*** **cumulative guggulsterone release from PCL-based microspheres over 44 days during the release study.**

Cumulative release was calculated from the total theoretical encapsulated guggulsterone per mg of microspheres in each sample replicate using the determined encapsulation efficiency value and the amount of guggulsterone leftover at each time point. Standard deviations are shown with a sample size of n=3.

3.2. Microsphere incorporation

Microspheres were incorporated with hiPSCs at a ratio of 0.5 mg of microspheres and 1 x 10^6 hiPSCs to form neural aggregates (**Fig. 9**). A couple hours after the cells and microspheres were deposited in the aggregate-forming wells, cell aggregates had already started to form in all test conditions. The incorporation of microspheres in the microsphere test condition was evident due to the dark spheroids inside of the aggregates visualized throughout the aggregate formation process and after attaching onto PLO/laminin plates. Although the successful incorporation of microspheres was observed, large microspheres (up to ~60 μm in diameter) beyond the expected average had been incorporated as well. Both the positive and negative control conditions lacked these dark spheroids as no microspheres were incorporated into them (**Fig. 9**). All test conditions displayed uniform spherical aggregate morphology at the end of 5 days. After attaching onto PLO/laminin plates and growing until day 15, the positive and negative control conditions seem to exhibit a more spread out aggregate center compared to the microsphere-incorporated aggregates with a lack of spreading of the microspheres themselves.

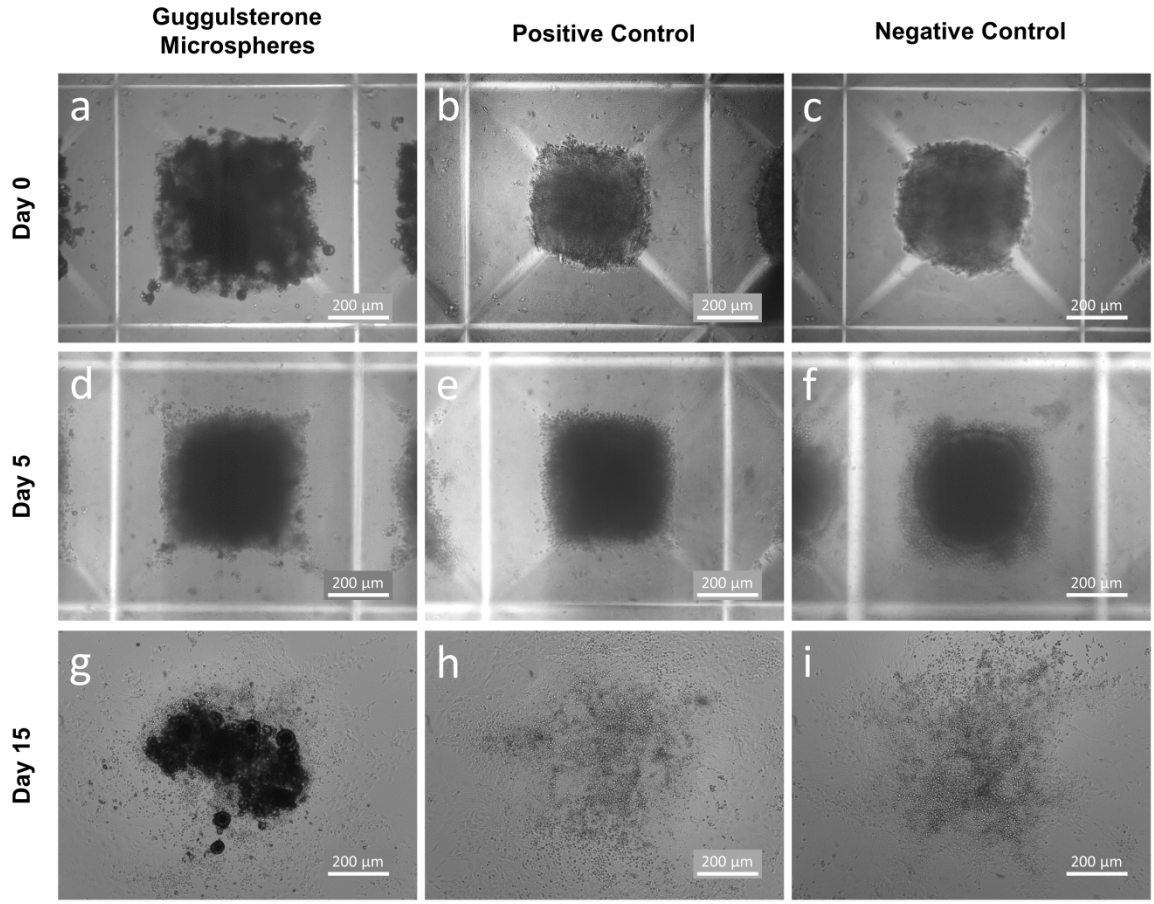

Figure 9. Bright field images of neural aggregate formation with Aggrewell plates.

Neural aggregate formation with (a) incorporated guggulsterone microspheres, (b) positive control soluble guggulsterone added to the media, (c) and negative control media taken at (a, b, c) day 0 and (d, e, f) day 5. (g, h, i) Growth and spreading of (g) a guggulsterone microsphere-incorporated neural aggregate, (h) a positive control neural aggregate, and (i) a negative control neural aggregate after 15 days. Neural aggregates were harvested and attached onto PLO/laminin culture plates on day 5. Guggulsterone microspheres are viewed as dark spheroids within the neural aggregates.

3.3 Immunocytochemistry

After 12 days *in vitro*, 7 days after attachment on PLO/laminin plates, the neural aggregates exhibited neurite outgrowth from the center of the aggregate in all test conditions and stained positive for beta-tubulin III (**Fig. 10**, **Fig.11**, **Fig. 12**). The microsphere-incorporated neural aggregates displayed a more spherical and less spread aggregate center with long neurites extending from this center (**Fig. 10**). Compared to the positive and negative control neural aggregates (**Fig. 11**, **Fig. 12**), the aggregate centers of the microsphere-incorporated test condition were difficult to visualize and single cell nuclei were difficult to resolve. In these aggregates, microspheres were identified by the presence of large dark spots in the staining. In contrast, positive and negative control aggregate centers exhibited dense collections of single cell nuclei with the presence of neural rosette structures and no microsphere indicative dark spots. Similar to the microsphere-incorporated condition, both positive control and negative control also exhibited beta-tubulin III positive neurites extending from the aggregate center, however, the negative control displayed a shorter and less dense morphology.

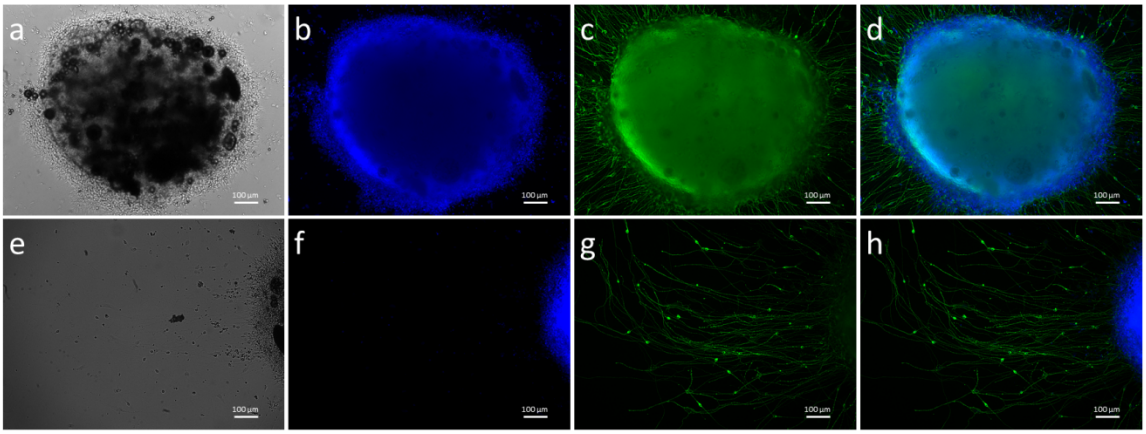

Figure 10. Immunocytochemistry images of a neural aggregate containing guggulsterone microspheres after 12 days *in vitro*.

(a) Bright field image showing microsphere incorporation (dark spheroids inside the aggregate). Fluorescence image of an aggregate stained with (b) DAPI for nuclei counterstaining, (c) βIII-tubulin for staining immature neurons, and (d) a composite image of fluorescence staining. (e-h) Immunohistochemistry images of neurites extending from the neural aggregate after 12 days *in vitro*. (e) Bright field, (f) DAPI staining, (g) βIII-tubulin, (h) fluorescence staining composite image of neurites.

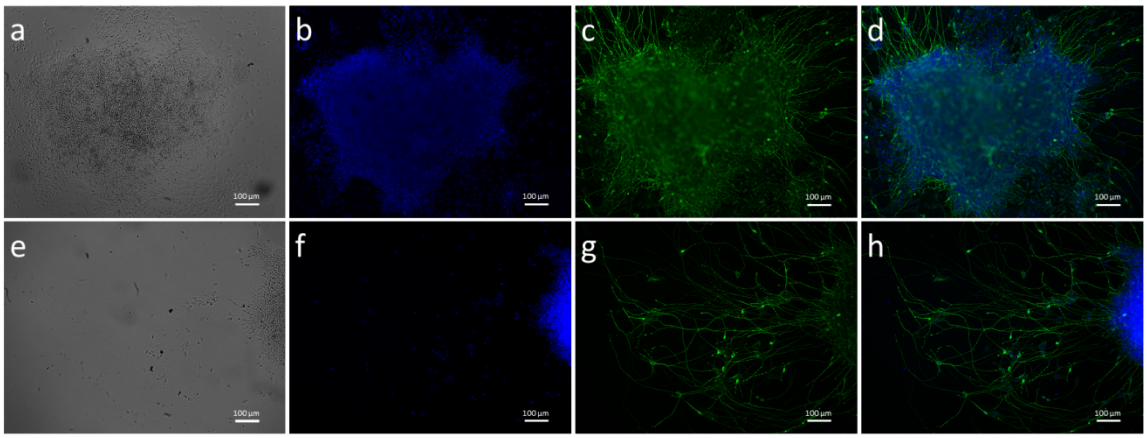

Figure 11. Immunocytochemistry images of a positive control neural aggregate after 12 days *in vitro* with soluble guggulsterone added to the media.

(a) Bright field image of the aggregate showing growth and spreading. Fluorescence image of an aggregate stained with (b) DAPI for nuclei counterstaining, (c) βIII-tubulin for staining immature neurons, and (d) a composite image of fluorescence staining. (e-h)

Immunohistochemistry images of neurites extending from the neural aggregate after 12 days *in vitro*. (e) Bright field, (f) DAPI staining, (g) βIII-tubulin, (h) fluorescence staining composite image of neurites.

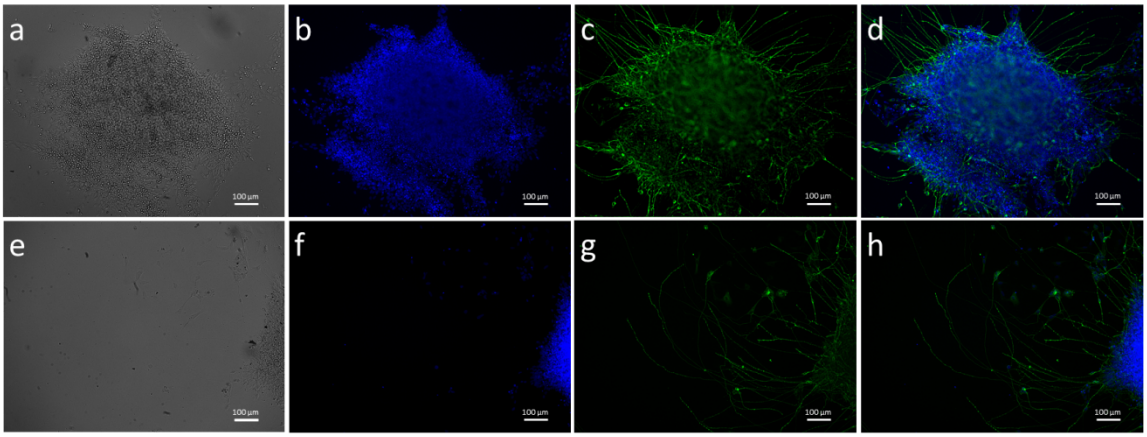

Figure 12. Immunocytochemistry images of a negative control neural aggregate after 12 days *in vitro*.

(a) Bright field image of the aggregate showing growth and spreading. Fluorescence image of an aggregate stained with (b) DAPI for nuclei counterstaining, (c) βIII-tubulin for staining immature neurons, and (d) a composite image of fluorescence staining. (e-h) Immunohistochemistry images of neurites extending from the neural aggregate after 12 days *in vitro*. (e) Bright field, (f) DAPI staining, (g) βIII-tubulin, (h) fluorescence staining composite image of neurites.

After 20 days of *in vitro* culture, 15 days after attachment on PLO/laminin plates, the neural aggregates exhibit extensive neurite outgrowth from the center of the aggregate in all test conditions and stained positive for beta-tubulin III (**Fig. 13**, **Fig.14**, **Fig. 15**). Again, the microsphere-incorporated neural aggregates displayed a more restricted aggregate center with dark spots from the presence of microspheres, however in comparison to day 12, the aggregates exhibit long-thick neurite bundles in a much denser arrangement extending from the center (**Fig. 13**). Similar to day 12, the positive and

negative control neural aggregate centers (**Fig. 14**, **Fig. 15**) exhibited collections of single cell nuclei with the presence of larger circular neural rosette structures and no microsphere-indicative dark spots. Similar to the microsphere-incorporated condition, both positive control and negative control also exhibited long and thick neurite morphology in a denser arrangement than day 12.

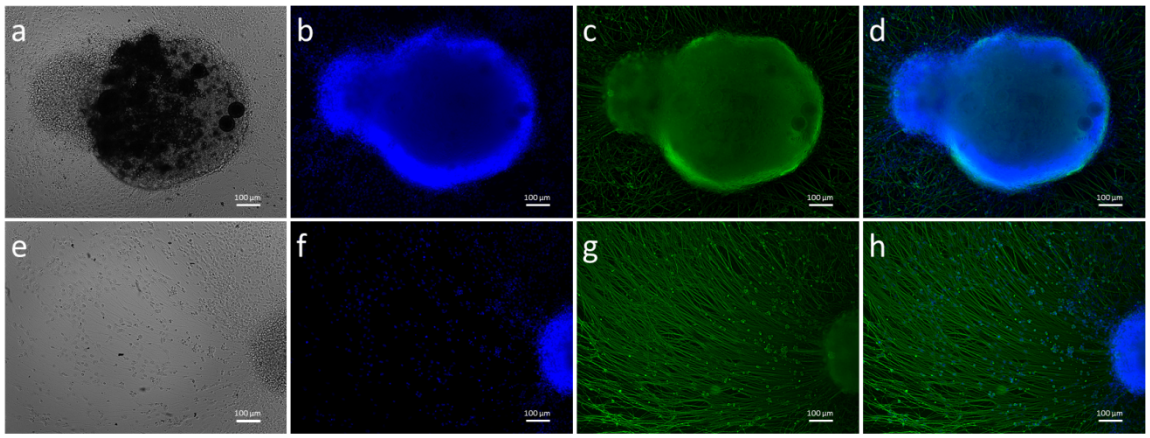

Figure 13. Immunocytochemistry images of a neural aggregate containing guggulsterone microspheres after 20 days *in vitro*.

(a) Bright field image showing microsphere incorporation (dark spheroids inside the aggregate). Fluorescence image of an aggregate stained with (b) DAPI for nuclei counterstaining, (c) βIII-tubulin for staining immature neurons, and (d) a composite image of fluorescence staining. (e-h) Immunohistochemistry images of neurites extending from the neural aggregate after 12 days *in vitro*. (e) Bright field, (f) DAPI staining, (g) βIII-tubulin, (h) fluorescence staining composite image of neurites.

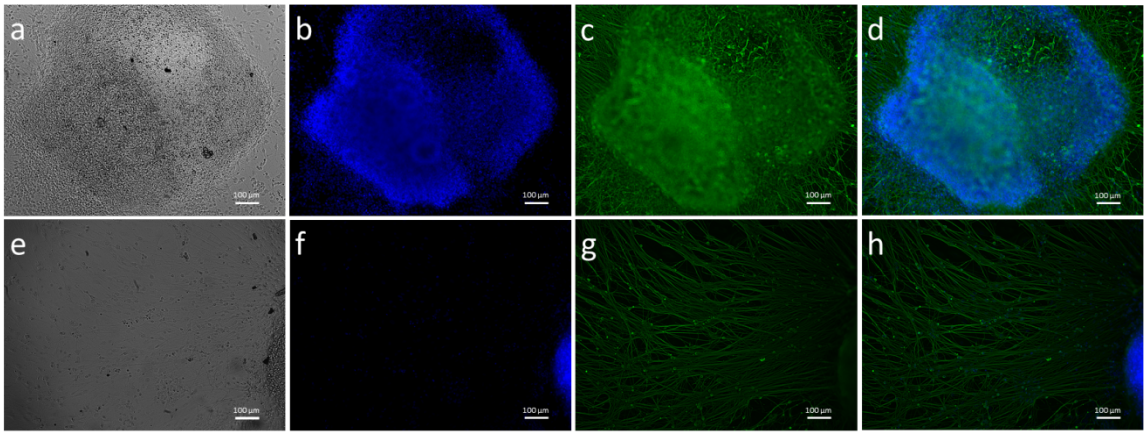

Figure 14. Immunocytochemistry images of a positive control neural aggregate after 20 days *in vitro* with soluble guggulsterone added to the media.

(a) Bright field image of the aggregate showing growth and spreading. Fluorescence image of an aggregate stained with (b) DAPI for nuclei counterstaining, (c) βIII-tubulin for staining immature neurons, and (d) a composite image of fluorescence staining. (e-h) Immunohistochemistry images of neurites extending from the neural aggregate after 12 days *in vitro*. (e) Bright field, (f) DAPI staining, (g) βIII-tubulin, (h) fluorescence staining composite image of neurites.

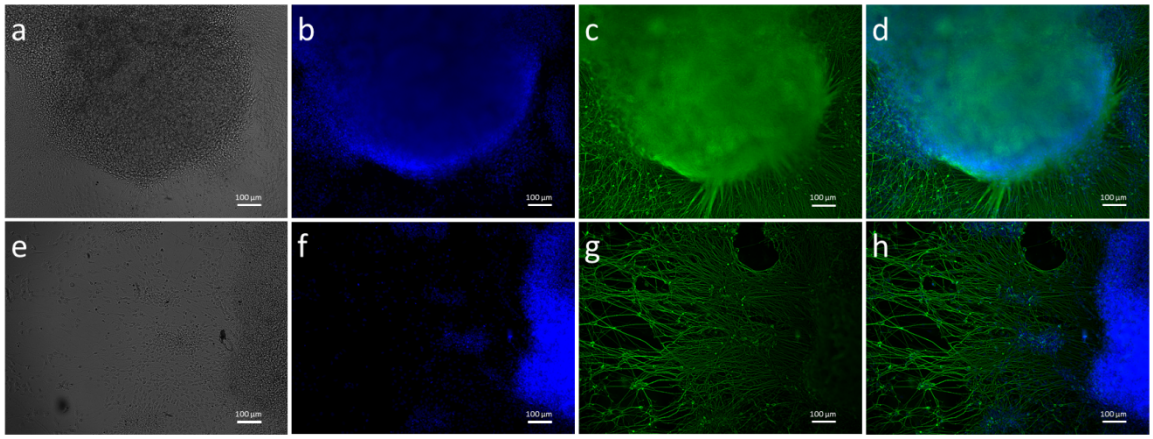

Figure 15. Immunocytochemistry images of a negative control neural aggregate after 20 days *in vitro*.

(a) Bright field image of the aggregate showing growth and spreading. Fluorescence image of an aggregate stained with (b) DAPI for nuclei counterstaining, (c) βIII-tubulin for staining immature neurons, and (d) a composite image of fluorescence staining. (e-h) Immunohistochemistry images of neurites extending from the neural aggregate after 12

days *in vitro*. (e) Bright field, (f) DAPI staining, (g) βIII-tubulin, (h) fluorescence staining composite image of neurites.

The composite stained images of the entire neural aggregates present similar data (**Fig.16** – **Fig. 21**). For day 12 neural aggregates, all conditions exhibited beta-tubulin III positive neurites (**Fig.16**, **Fig. 17**, **Fig. 18**). Again, the microsphere-incorporated aggregate displayed a restricted center difficult to resolve for finer elements within while the negative control aggregates had a sparse number of neurites compared to the microsphere-incorporated and positive control conditions. Quantitatively, the microsphere-incorporated aggregate condition did not have enough replicates to draw any conclusions from, however, the positive control was calculated to have longer neurites and more neurite branching than the negative control on day 12 (**Fig. 22**). Although the neurite metrics for the positive control were higher than the negative control on day 12 as displayed with standard deviations in **Fig. 22**, there was no statistical significance calculated due to the low number of replicates ($n=2$, $p = 0.172$ for neurite length and $p = 0.149$ for neurite branching). Neural aggregates in all three conditions exhibited extensive neurite outgrowth by day 20. Again, the only qualitative difference was the restricted center of the microsphere-incorporated aggregate. At the end of the *in vitro* study, the neurite metrics on day 20 yielded no significant difference between positive control and negative control neurite length or neurite branching (**Fig. 23**).

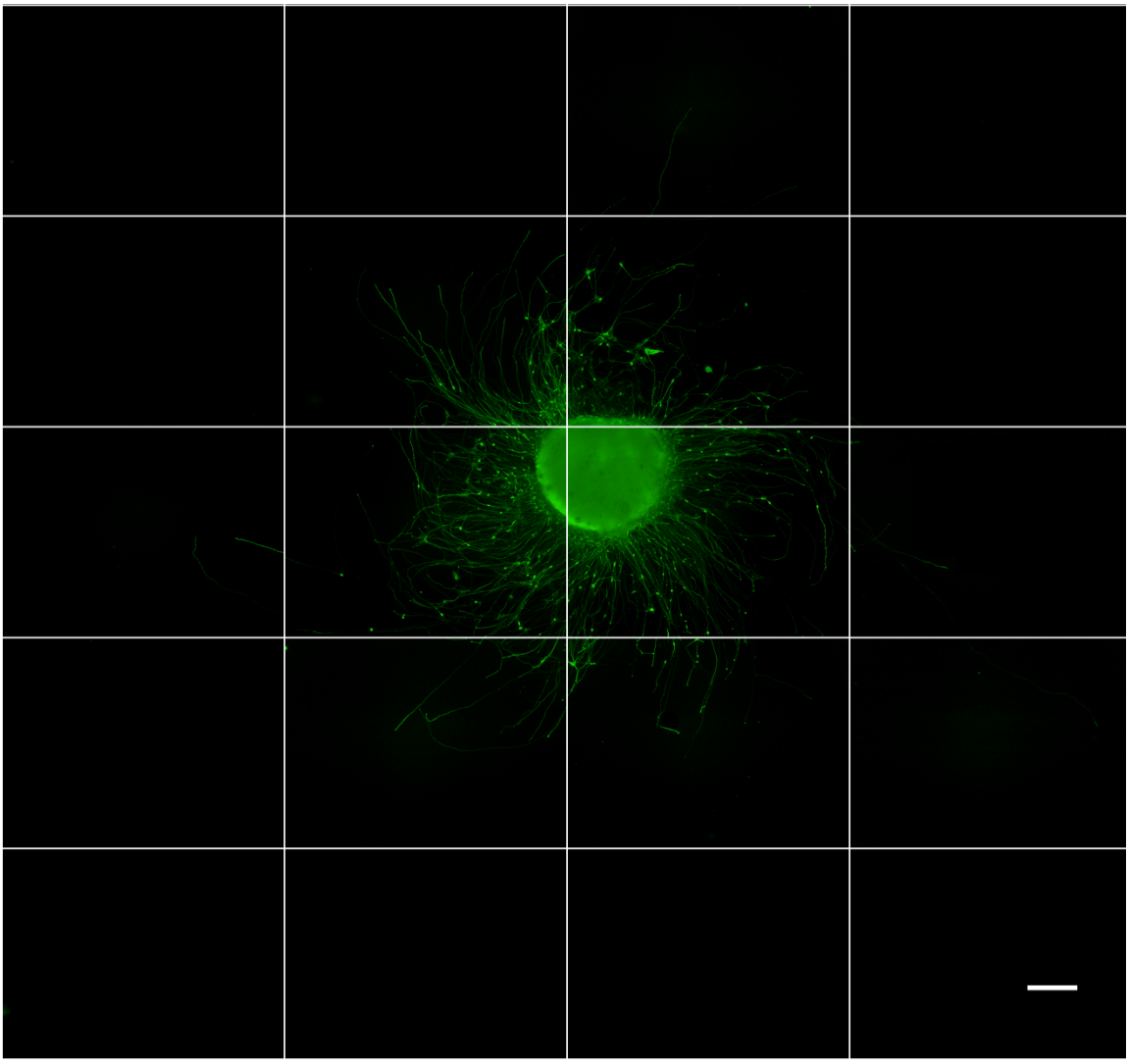

Figure 16. Fluorescence image of a neural aggregate containing guggulsterone microspheres after 12 days *in vitro*.

The aggregate was stained with βIII-tubulin for immature neurons and shows neurite branching extending out from the aggregate. Incorporated microspheres are viewed as dark spheroids inside of the aggregate. The image was compiled from 36 separate images taken by an IncuCyte automatic imaging machine and stitched together and cropped with ImageJ software. Scale bar represents 300 μm.

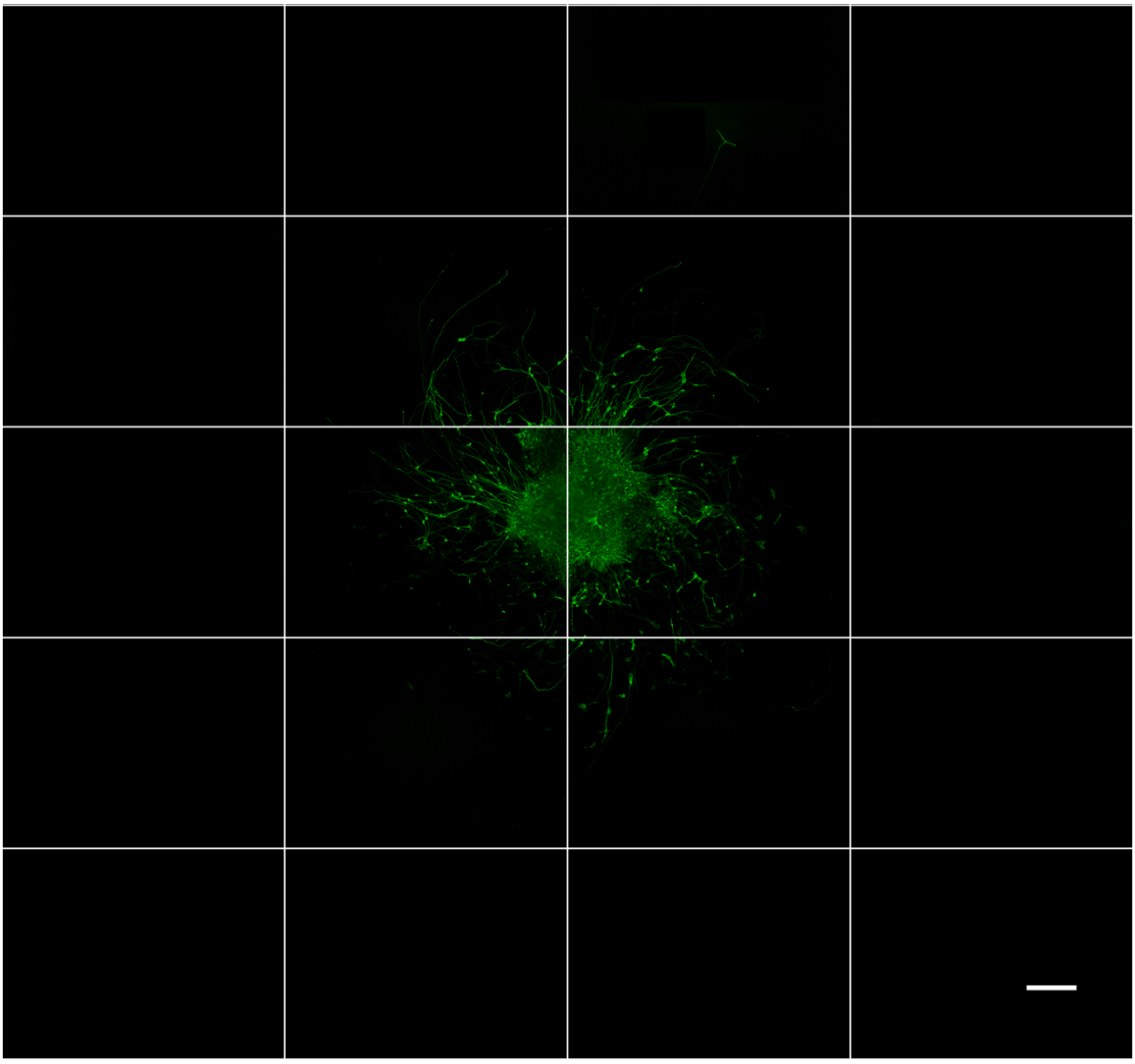

Figure 17. Fluorescence image of a positive control neural aggregate after 12 days *in vitro* with soluble guggulsterone added to the media.

The aggregate was stained with βIII-tubulin for immature neurons and shows neurite branching extending out from the aggregate. The image was compiled from 36 separate images taken by an IncuCyte automatic imaging machine and stitched together and cropped with ImageJ software. Scale bar represents 300 μm.

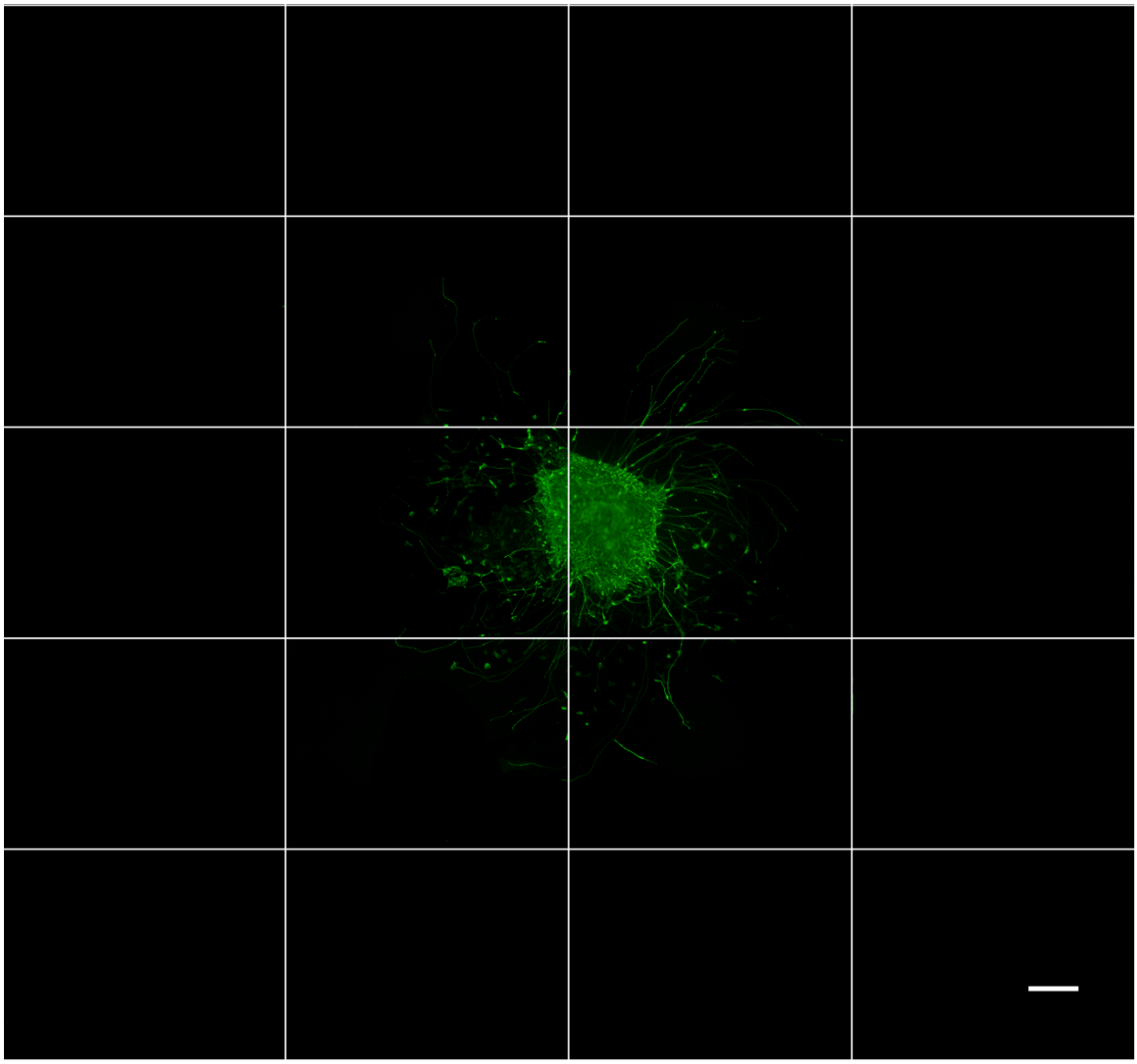

Figure 18. Fluorescence image of a negative control neural aggregate after 12 days *in vitro*. The aggregate was stained with βIII-tubulin for immature neurons and shows neurite branching extending out from the aggregate. The image was compiled from 36 separate images taken by an IncuCyte automatic imaging machine and stitched together and cropped with ImageJ software. Scale bar represents 300 μm.

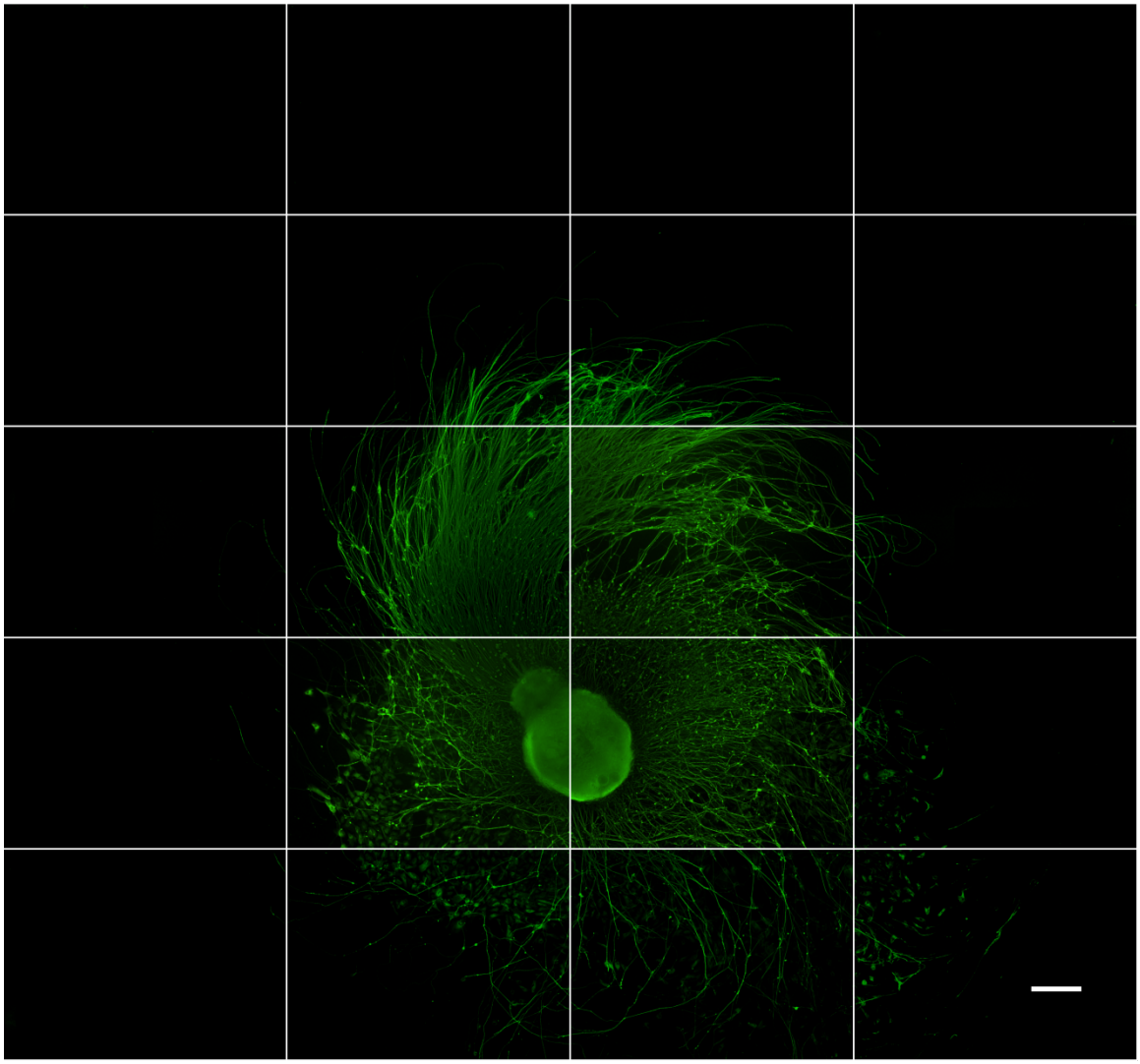

Figure 19. Fluorescence image of a neural aggregate containing guggulsterone microspheres after 20 days *in vitro*.

The aggregate was stained with βIII-tubulin for immature neurons and shows neurite branching extending out from the aggregate. Incorporated microspheres are viewed as dark spheroids inside of the aggregate. The image was compiled from 36 separate images taken by an IncuCyte automatic imaging machine and stitched together and cropped with ImageJ software. Scale bar represents 300 μm.

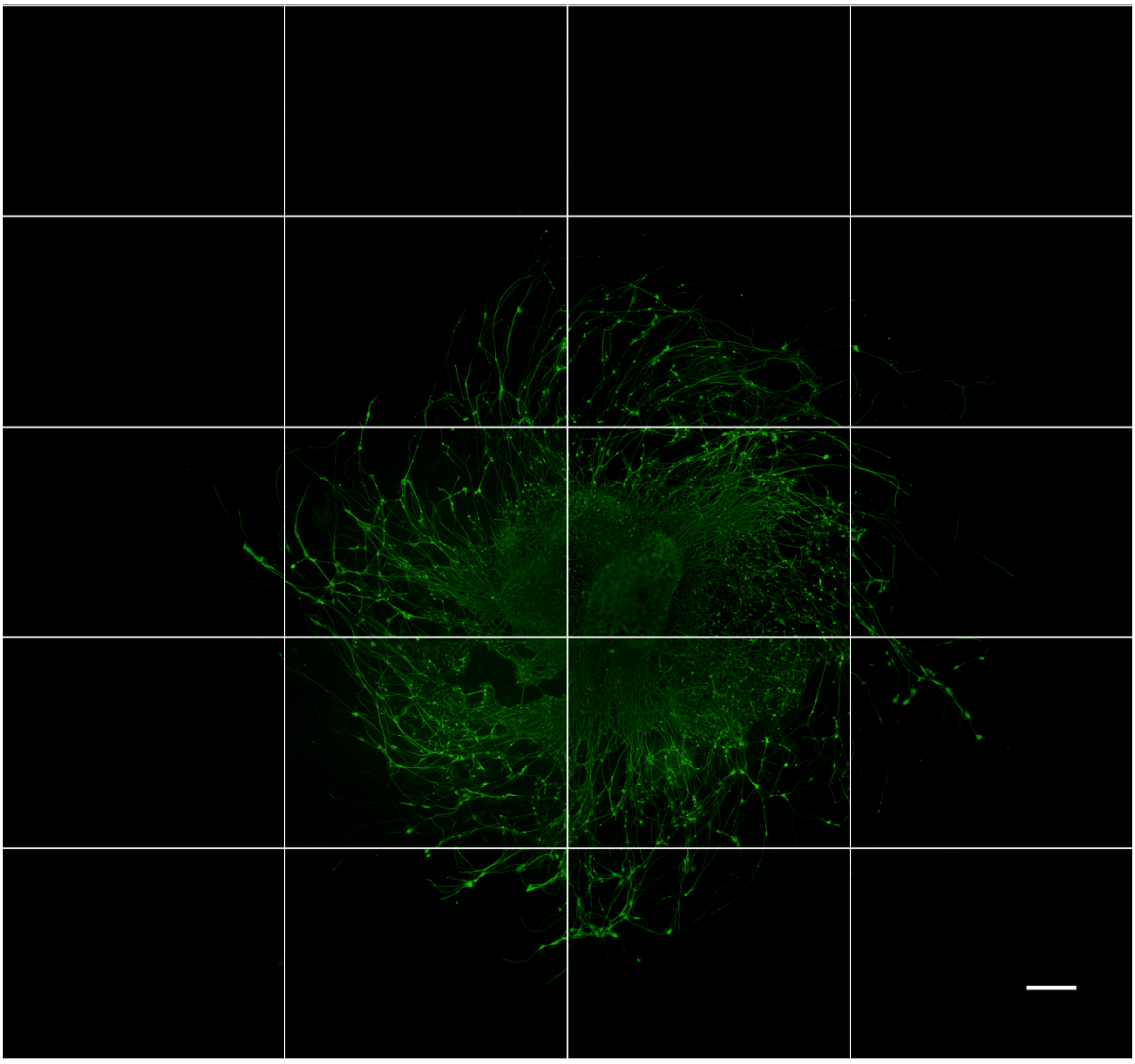

Figure 20. Fluorescence image of a positive control neural aggregate after 20 days *in vitro* with soluble guggulsterone added to the media.

The aggregate was stained with βIII-tubulin for immature neurons and shows neurite branching out from the aggregate. The image was compiled from 36 separate images taken by an IncuCyte automatic imaging machine and stitched together and cropped with ImageJ software. Scale bar represents 300 μm.

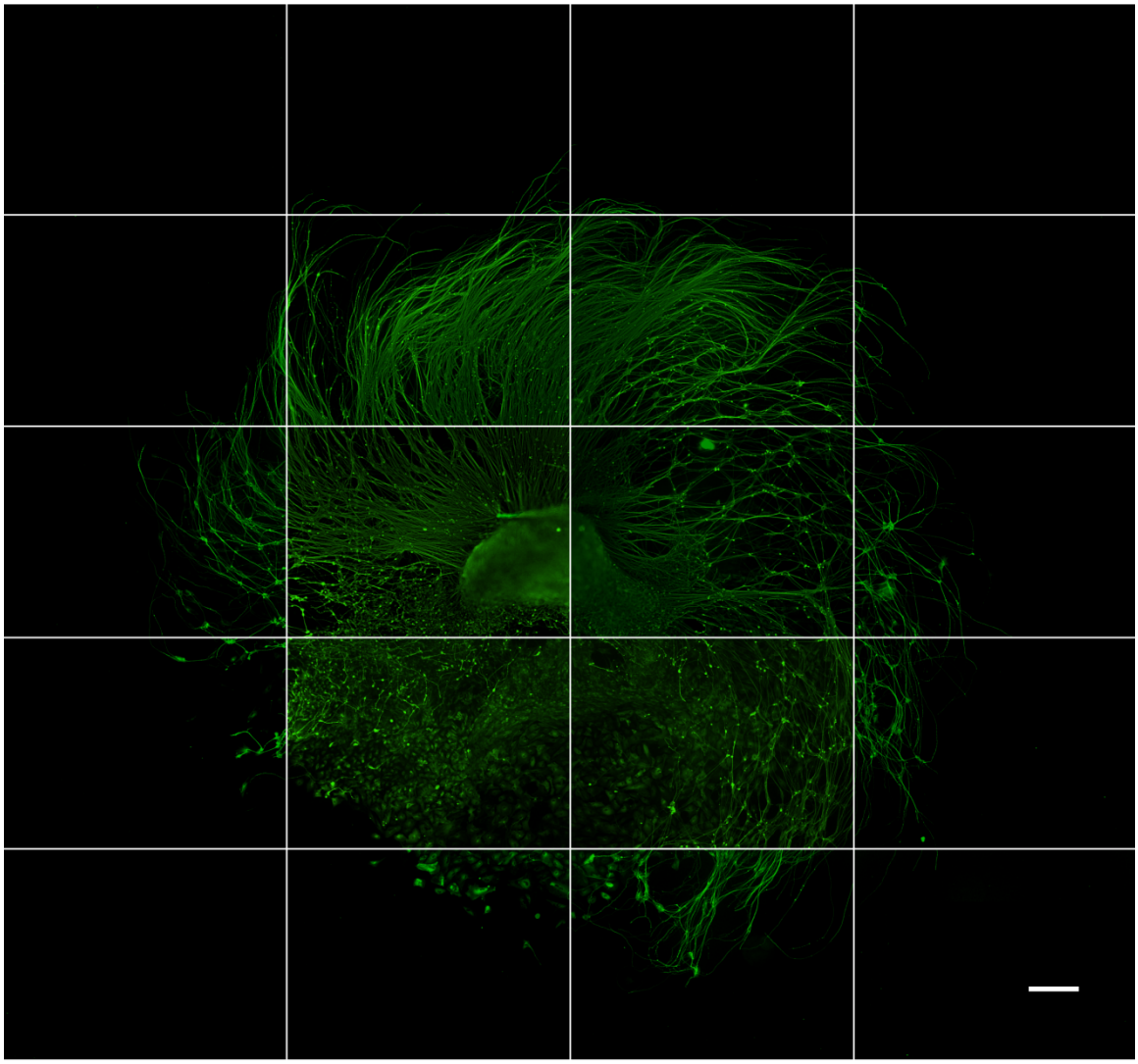

Figure 21. Fluorescence image of a negative control neural aggregate after 20 days *in vitro*. The aggregate was stained with βIII-tubulin for immature neurons and shows neurite branching out from the aggregate. The image was compiled from 36 separate images taken by an IncuCyte automatic imaging machine and stitched together and cropped with ImageJ software. Scale bar represents 300 μm.

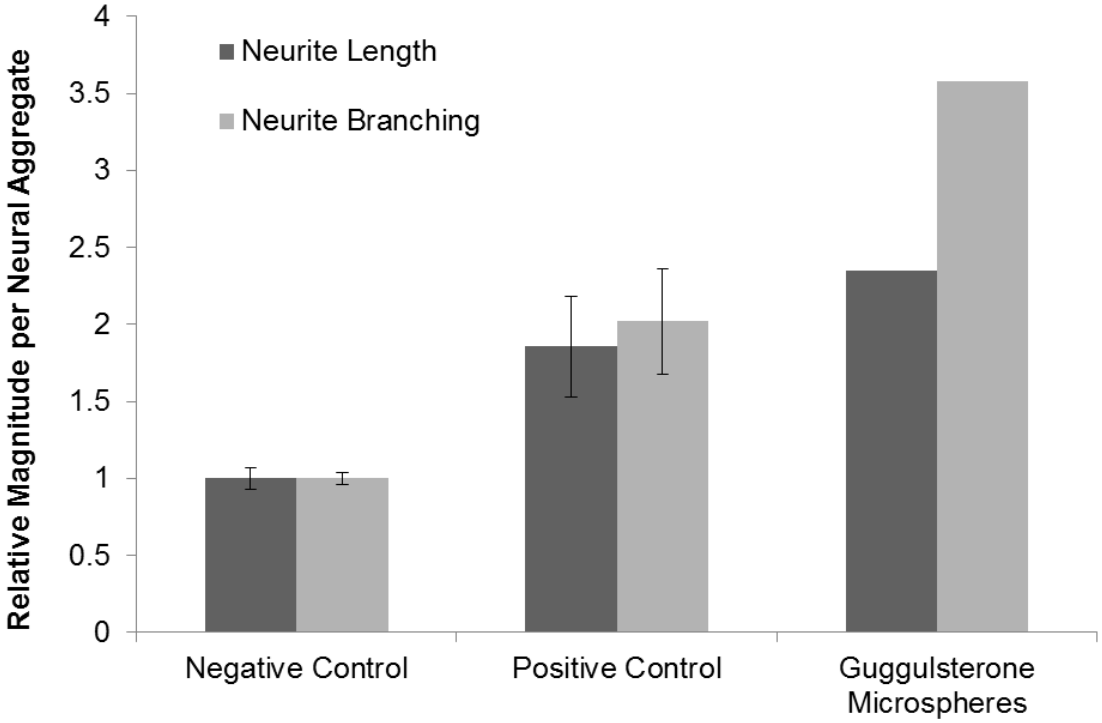

Figure 22. Quantitative analysis of neural aggregate morphology for neurite length and branching after 12 days *in vitro*.

The negative control neural aggregates (n=2) were used to normalize the data against the positive control (n=2) and guggulsterone microsphere-incorporated (n=1) aggregates. Neurite length and neurite branching were both calculated per cell cluster area. Cell morphology metrics were identified and quantified by an IncuCyte ZOOM® live-cell imaging system using the Neurotrack and Basic Analyzer cell masking software. Standard deviations are shown.

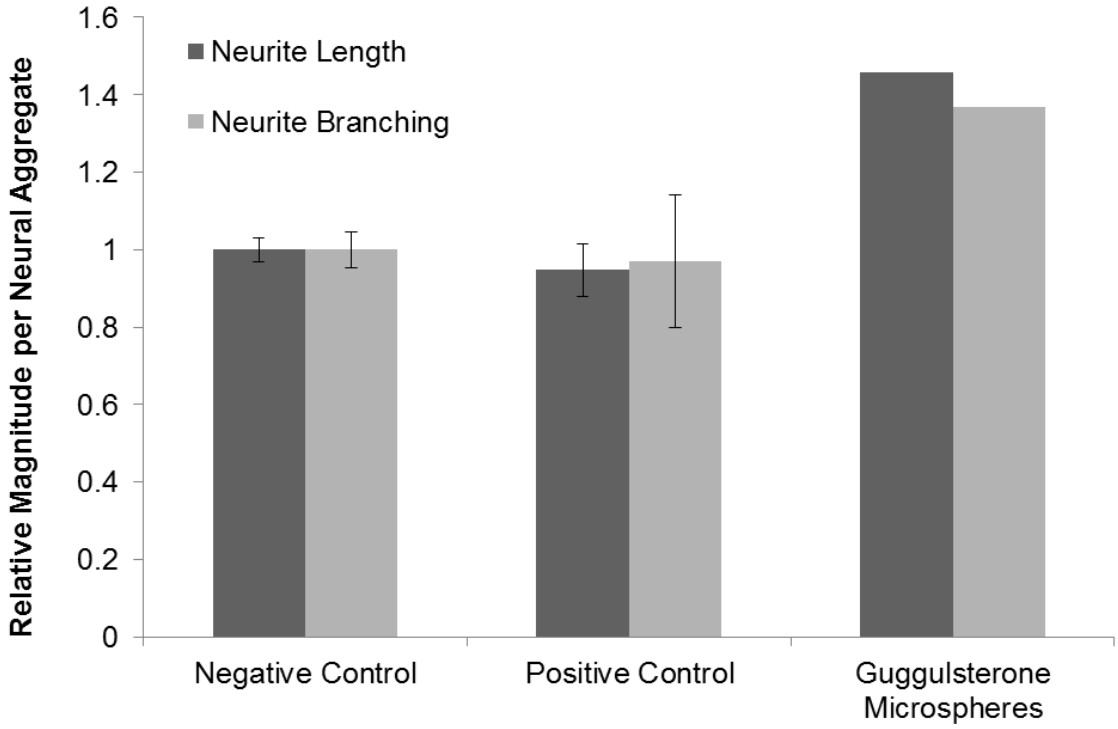

Figure 23. Quantitative analysis of neural aggregate morphology for neurite length and branching after 20 days *in vitro*.

The negative control neural aggregates (n=2) were used to normalize the data against the positive control (n=2) and guggulsterone microsphere-incorporated (n=1) aggregates. Neurite length and neurite branching were both calculated per cell cluster area. Cell morphology metrics were identified and quantified by an IncuCyte ZOOM® live-cell imaging system using the Neurotrack and Basic Analyzer cell masking software. Standard deviations are shown.

Chapter 4 - Discussion

4.1. Microsphere characterization

Guggulsterone is a steroid molecule that promotes the terminal differentiation of DNs from PSCs (Gonzalez, et al., 2013). Although the molecule is a promising solution for replacing the cocktail of drugs currently recommended to produce DNs thereby making the protocol easier, cheaper, and simpler, there has been limited scope on the research of this drug for this purpose. In fact, there has been no published material on the controlled release of guggulsterone. In terms of providing a better way to produce such neurons, the use of a biodegradable microsphere system for the release of guggulsterone could allow long-term release to decrease the labour of daily media changes, decrease the amount of drug needed to differentiate the PSCs due to the high concentration needed when dissolved in media, and provide a method of extending terminal differentiation times *in vivo* through implantation. This study investigates a possible method of guggulsterone delivery for long-term release in the differentiation of PSCs.

In response to previous successful small molecule releasing drug delivery systems, single emulsion microspheres were chosen to encapsulate guggulsterone (Bratt-Leal, et al., 2011; Bratt-Leal, et al., 2013; Carpenedo, et al., 2009; Carpenedo, et al., 2010; Ferreira, et al., 2008; Gomez, et al., 2015; Qutachi, et al., 2013). Similarly, PCL was chosen for fabrication since it is an excellent polymer candidate for drug delivery at a low price and long-term degradation rate (Sinha, et al., 2004; Woodruff & Hutmacher,

2010). As such, the encapsulation of guggulsterone within microspheres was demonstrated.

Previous parameters for fabricating double emulsion and single emulsion microspheres were used to produce microspheres with a small diameter and spherical morphology (Agbay, et al., 2014; Gomez, et al., 2015). Although producing microspheres less than 10 μm was achieved, the size distribution of the microspheres was not uniform. The histogram and diameter averages suggest a varied size distribution. There is a large percentage of microspheres under 10 μm, however, there is also a low number of microspheres at much larger diameters. This is reflected in the large standard deviation of 9.09 μm through hand measuring which is around a third larger than the average itself (6.14 μm). Although particle-sizer analysis yielded an average that resides within the large standard deviation of the hand-measured value, its average is more than twice the diameter and resulted in a smaller standard deviation (14.8 ± 5.9 μm). Here, a non-homogeneous size distribution may have contributed to the possibility of larger microspheres in the particle-sizer samples which could have inflated the average. In addition, the difference between hand-measured and particle-sizer averages may be due to the particle sizer having difficulties with measuring a non-uniform sample of molecules which tend to settle out in solution. As such, it may be more correct to refer to the median (3.28 μm) of the hand-measured values to estimate the size of the microspheres. In any case, it would be helpful to constrict the size distribution of the fabricated microspheres in the future. Possible methods include filtering the microspheres to exclude microspheres larger than a specified size, fabricating microspheres with a microfluidic system to have more acute control of the emulsion process (Zhao, 2013), or

differential centrifugation to pellet out different sized microspheres at different speeds (Dutta, Salifu, Sirianni, & Stabenfeldt, 2015).

The encapsulation efficiency reflects the amount of guggulsterone encapsulated in the microspheres compared to the amount of the drug added during the fabrication process. Not only does it represent the amount of drug wasted during fabrication but it also affects the amount of drug released. The encapsulation efficiency was determined to be almost half of the drug added at 42.4 ± 3.5 %. This is similar, albeit slightly lower than retinoic acid encapsulated microspheres previously published with similar fabrication parameters (~48-58%) (Gomez, et al., 2015; Jeong et al., 2003). Since the parameters used to produce the guggulsterone microspheres were similar to these studies and resulted in a lower encapsulation efficiency, it is possible that the structure of the drug is the reason for this decrease in loading (Gomez, et al., 2015). Guggulsterone is a steroid molecule mainly consisting of the signature cholesterol four hydrocarbon ring whereas the previous studies encapsulated the drug retinoic acid composed of a single cyclic ring structure with a hydrocarbon chain. Older studies of steroid molecule encapsulation in single emulsion microspheres report encapsulation efficiencies as low as ~9% for hydrocortisone (Giunchedi, Alpar, & Conte, 1998), ~22% for levonorgestrel (L. R. Beck, Pope, Tice, & Gilley, 1985), and ~55% being the highest for hydrocortisone 21-acetate (Giunchedi, et al., 1998). In these studies, it is apparent that organic solvent solubility may affect encapsulation efficiency. Hydrocortisone had an encapsulation efficiency of 9% while its more soluble ester hydrocortisone 21-acetate exhibited 55% efficiency (Giunchedi, et al., 1998). Indeed, the increasing solubility of levonorgestrel, guggulsterone, and retinoic acid in ethanol is consistent with their reported relative

encapsulation efficiencies (~22%, ~42%, and ~60%, respectively). Another possible reason for the decrease in encapsulation may be the drug extraction method. Due to the nature of the chosen HPLC analysis, an altered method of extracting the drug from microspheres was used to determine encapsulation efficiency. Previously, DCM was used to dissolve the microspheres completely in order to extract drug into another organic solvent. In fact, the altered method utilized ACN, an organic solvent in which PCL is less soluble, to dissolve the microspheres. It may be possible that during the drug extraction process, the microspheres were not completely dissolved and the resulting drug extracted for encapsulation efficiency determination was not the entire amount encapsulated within the microspheres. Adjusting the drug extraction method by increasing the temperature of the system or lengthening the time to dissolve the polymer may yield higher encapsulation efficiencies.

The release kinetics of guggulsterone from the microspheres was observed over 44 days to parallel and surpass the terminal 38 day differentiation treatment of guggulsterone in the previous hiPSC study (Robinson, et al., 2015). In terms of cumulative release, the rate of drug release is similar to the previous PCL single emulsion microsphere system fabricated by Gomez et al. (Gomez, et al., 2015). In fact, at day 28 the release of guggulsterone was ~45% of the total drug encapsulated which is similar to retinoic acid release from PCL microspheres at ~ 28% and ~53% for two different concentrations (the latter concentration being 7.5 times greater than the former) (Gomez, et al., 2015). These results confirm our expectations for producing microspheres with a guggulsterone release time course greater than 38 days using PCL. According to the study by Gomez et al., it can also be surmised that changing the concentration of drug

added to the fabrication process may affect the rate of release, increasing cumulative release in a shorter length of time with increasing drug concentration (Gomez, et al., 2015). Furthermore, since only ~62% of the drug has been released from the microspheres at the end of the 44 day release study, additional release of the remaining drug is possible which can be advantageous for promoting terminal differentiation. Although in contrast to double emulsion microspheres where you can see a plateau in cumulative release, similar to other single emulsions the cumulative release of the guggulsterone microspheres displays a more linear profile with additional release of the drug still predicted to happen. If the rate of release continues to be consistent beyond 44 days, releasing the remaining drug would take an estimated 27 days for a total of 71 days of drug release.

The average release of guggulsterone per day from ~10 mg of microspheres was calculated to be ~37 ng. In the case of incorporation with hiPSCs, 0.5 mg of microspheres were added to each aggregate forming well at the suggestion of a previous study to keep aggregates intact (Gomez, et al., 2015). This would correspond to a concentration of ~0.93 ng/mL of guggulsterone released from 0.5 mg of microspheres. In comparison, Robinson et al. added guggulsterone at a concentration of 2.5 μM corresponding to a concentration of 781 ng/mL in each aggregate forming well (Robinson, et al., 2015). Accordingly, the determined release from the microspheres is not sufficient to match the drug concentrations outlined in previous DN-producing guggulsterone studies (Gonzalez, et al., 2013; Robinson, et al., 2015). However, the concentrations used in these studies are not confirmed to be the effective concentrations required to elicit differentiation of PSCs into DNs and it is likely that such an effective concentration is lower than what is

outlined. To date, no study has determined the effective concentration of guggulsterone for such applications. As previously stated, these guggulsterone-releasing microspheres can be fabricated with a higher concentration of drug encapsulated to increase release per day in exchange for a shorter release period. Finally, microspheres allow drug release inside of cellular aggregates which may create a more homogenous local delivery of the drug. In contrast, soluble drug in the media may produce a decreasing concentration gradient of the drug towards the center of the aggregate. Since there are concerns of mass transfer limitations inside of cell aggregates (Van Winkle, et al., 2012) and evidence of aggregate structural changes that restrict diffusive transport (Sachlos & Auguste, 2008), it may be possible that the drug concentrations required for release from microspheres are lower than media soluble drug concentrations for the same differentiation induction effect. In fact, Ferreira et al. has previously reported that lower concentrations of the vascular differentiation factors bFGF and PIGF released from PLGA microspheres resulted in comparable or even superior vascular differentiation through incorporation into EBs vs. soluble drug in media (bFGF at 175 pg/mL vs. 50 ng/mL and PIGF at 887 pg/mL vs. 50 ng/mL) (Ferreira, et al., 2008). In this study, vascular differentiation could be achieved from microsphere release at concentrations much lower than the concentrations of soluble drug in media.

4.2. Microsphere incorporation and immunocytochemistry

Incorporation of microspheres within neural aggregates appeared to be successful. It may be useful to ensure that the dark spheres in the aggregates are in fact microspheres by detecting their chemical composition with transmission electron microscopy.

Nonetheless, after 5 days in the aggregate-forming wells, the cell aggregates did not disintegrate and kept their spherical structure when attaching on PLO/laminin plates, although there were large microspheres (up to ~ 60 μm) incorporated. However, these large incorporated microspheres may have had an effect on the observed morphology of the aggregates. It was evident that the positive and negative control aggregates seemed to spread out more after attaching onto PLO/laminin plates. Perhaps the large microspheres had prevented spreading as cells may have attached to their surfaces tethering other cells nearby. The polymer PCL does not readily support cell attachment due to its lack of functional groups and inherent hydrophobicity, however, surface modifications have been used to change this property (Atyabi et al., 2016; Bramfeldt & Vermette, 2009; Chung, Wang, Wang, Hsieh, & Fu, 2009; Recek et al., 2016; Yildirim et al., 2010). Among these modifications, plasma treatment has been found to increase cellular adhesion on the polymer surface (Atyabi, et al., 2016; Recek, et al., 2016; Yildirim, et al., 2010). For the cellular *in vitro* portion of this study, the use of plasma sterilization on the microspheres before incorporation may have imparted a similar increased adhesion property to the polymer and the large surface area of the microspheres may have affected the aggregate's ability to spread out. To study the possible effects of microspheres alone, it would be useful to incorporate blank microspheres without encapsulated drug with the cells as well.

Similarly, such large objects incorporated inside of the aggregates may have also prevented the formation of neural rosettes as evidenced by the lack of ring like structures within microsphere-incorporated aggregates. Neural rosette structures are a developmental signature indicating the production of NPCs derived from ESCs akin to

development of the neural tube in embryos (Wilson & Stice, 2006). It is unclear whether neural rosettes were prevented from forming due to the large microspheres, the rosettes lifted off of the aggregate and into the media, or if the microspheres simply affected the staining of the aggregate leading to the inability to resolve finer structures in the center of the aggregate. If indeed the large microspheres affected neural rosette formation, it would most likely have detrimental effects on neuronal differentiation. Confining the microspheres to a smaller size distribution would be essential for incorporation in the future. In any case, conclusions about the state of differentiation of the neural aggregates between conditions were difficult to make as the only marker stained for was beta-tubulin III a general neuronal marker. Staining with a mature marker such as NeuN for postmitotic neurons would provide further evidence for the extent of mature neuron differentiation between conditions. In addition to this, staining for other neural markers (GFAP for astrocytes and Olig2 for oligodendrocytes) would provide information on the differentiation into unwanted phenotypes and secondary antibody stain controls should be done to confirm the lack of unspecific binding fluorescence.

Beta-tubulin III staining was present in the neurites of all conditions as expected due to the production of neural-ectodermal fated cells by the use of NIM. Differences in staining are then assumed to be differences in cell maturity or neural cell type. As expected, from day 12 to day 20 the number of neurites increased as well as their length, branch points, and complexity of arrangement. Quantitative comparisons for this result could not be made since the processing definition for masking neurites and cell bodies were not the same for each time point. This was due to the day 20 images having a more complicated morphology and a more homologous fluorescence across neurites and

aggregate center to make it difficult for the software to separate objects with the same definition as day 12 images. Similarly, quantitative comparisons between treatments for the same time point could not be made due to the low number of replicates (n=2 for positive and negative control, n=1 for microsphere-incorporated treatment). However, the images suggest neurite length and branching for the negative control condition on day 12 were less than the positive control on day 12. Although statistical significance could not be calculated due to the low number of replicates (n=2), the graphical representation of the means and standard deviations suggest a significant difference if additional replicates should be added in the future. This perceived difference did not persist to day 20 as the negative control and positive control neurite metrics were similar at the final time point.

It is still unclear how guggulsterone affects signalling pathways for dopaminergic differentiation and revealing such information could help explain this difference in early neurite growth. In addition, introduction of the drug at the outset of differentiation rather than at terminal differentiation has not been studied before. Although this study is an initial test of compatibility of guggulsterone-releasing microspheres with hiPSCs, delivering guggulsterone throughout differentiation instead of at the final stage may not be beneficial for producing DNs. It is clear that further studies investigating the role of guggulsterone on neuronal differentiation pathways must be done. If guggulsterone does in fact promote the differentiation of DNs during the entire differentiation process including early on, perhaps during early differentiation a larger number of cells quickly adopt a more neuron-like morphology maturing quicker beyond the neural progenitor stage in the presence of guggulsterone. This would explain the apparent increase in neurite length and branching of the positive control at day 12. Both positive and negative

control conditions exhibit neural rosette structures which indicate the presence of NPCs at day 12 and day 20. Without guggulsterone, the PSCs would still be induced to a neuronal lineage with NIM, however, a greater proportion of the cells may still be in a NSC or NPC stage. The positive control may have had more mature neurons at day 12. At day 20, cells in the negative control condition may have caught up to the guggulsterone-treated cells with a similar number of cells exhibiting neurite outgrowth and differentiation beyond the neural progenitor stage. Although the beta-tubulin III staining of neurites is similar in positive and negative control groups at day 20 to possibly reflect this, the guggulsterone-exposed group may have even more mature neurons at this point. In this case, a possible signalling target for guggulsterone may be the promotion of the Wnt/β-catenin pathway as it has been shown in early differentiation to enhance DN production efficiency as described by Kriks et al. (Castelo-Branco, et al., 2004; Castelo-Branco, et al., 2003; Kriks, et al., 2011).

Conversely, guggulsterone may not promote a specific pathway that directs differentiation to a dopaminergic fate but may inhibit a pathway that directs the differentiation to another cell type. Signal transducers and activator of transcription 3 (STAT3) is a transcription factor implicated in the growth of tumor cells and is constituatively active in in many human cancer cells (Buettner, Mora, & Jove, 2002). As previously mentioned, guggulsterone has been studied as a drug for the treatment of cancer and there has been evidence suggesting that it does so by inhibiting STAT3 signalling (Ahn et al., 2008). Interestingly, the STAT3 pathway is also required for the differentiation of astrocytes and is a main mechanism for promoting astogenesis (Hong & Song, 2014; Wen, Li, & Liu, 2009). Perhaps the increase in efficiency of dopaminergic

differentiation reported by Gonzalez et al. and the suggested increase in early neurite growth in this study may be due to the inhibition of the STAT3 pathway by guggulsterone causing a decrease in astrocyte production and an increase in neuron yield (Gonzalez, et al., 2013).

Although DN replacement therapy for the treatment of PD is a step towards a more complete treatment of the disease, there are a number of risks and potential obstacles. Since the molecular pathogenesis of PD is still currently unresolved, newly implanted DNs may still be susceptible to the disease. If this is the case, understanding the underlying pathogenesis of PD remains critical in stopping the progression of the disease and protecting newly implanted DNs. When identifying positive outcomes for neuronal differentiation studies, perhaps production of longer and more branched neurites, increased dopamine release, and generation of one specific type of neuron may not be ideal for implantation. Although careful observation of neuronal overgrowth is stressed during implant studies in animals, analysis of the extent of integration of neurons with existing cells should be emphasized as well. Additionally, dopamine release from a produced pool of neurons should be compared to physiological dopamine release from neurons *in vivo*. Eventually, the implantation of supportive glial cells alongside the target neuron replacement population may be necessary to recapitulate the neuronal environment in a healthy brain and lead to better functional outcomes.

4.3 Future directions

As previously stated, further staining with more mature markers such as NeuN and MAP2 for postmitotic neurons or flow cytometry tracking of immature neuronal

marker expression of Nestin and mature differentiation marker expression of SSEA1 would provide further evidence for the extent of neuronal maturity across time points. In addition, staining for astrocyte and oligodendrocyte markers would identify differentiation into unwanted phenotypes.

The confirmation of bioactivity of guggulsterone released from microspheres could not be determined due to time constraints. It was observed that guggulsterone-encapsulated microspheres were successfully incorporated into hiPSC-derived neural aggregates, however, the effect of guggulsterone release could not be resolved in the current study. Further experiments must look at duplicating the current neural aggregate formation study to gather more neurite metric data especially for the microsphere-incorporated condition and include flow cytometry data tracking neural lineage, pluripotency, and viability markers. Also, incorporation of microspheres without any drug encapsulated would help to determine the effect of guggulsterone released from the microspheres compared to the microspheres themselves.

It would be valuable to extend the time of the *in vitro* cell study to 57 days matching the duration of the study done by Robinson et al. to determine DN differentiation by tyrosine hydroxylase (DN marker) staining, use of dopamine enzyme-linked immunosorbent assays, and electrophysiology (Robinson, et al., 2015). Moreover, once compatibility with the hiPSC-derived cells are fully understood, incorporation of the guggulsterone-encapsulated microspheres at the terminal differentiation stage (day 19) after NPCs are treated with SHH and FGF8 should be done to directly compare the soluble treatment protocol with using microspheres for drug release.

Using guggulsterone-encapsulated microspheres in replacement of daily soluble

drug administration at the final stage of differentiation will determine the ability of the microspheres to produce DNs in a cheaper and more effective way. If the guggulsterone delivery system can be successful in this, future directions could be to integrate such drug delivery technology with bioreactors to decrease the concentration of drug needed in the continuously flowing media or to use the microspheres in the implantation of PSC-derived DNs to extend the terminal differentiation period *in vivo*. Along with the guggulsterone microspheres described in this study, previously encapsulated retinoic acid microspheres and continuing work on purmorphamine encapsulation will provide an opportunity to develop a modular drug delivery system with multiple types. If the effectiveness of the guggulsterone microspheres on influencing differentiation can be confirmed, developing different combinations of drug-releasing microspheres to produce neurons of different types according to microsphere ratios may be feasible in the future.

4.4 Conclusions

Guggulsterone is a promising drug for the terminal differentiation of DNs from PSCs. Here, I have encapsulated guggulsterone within PCL microspheres with a single emulsion technique and demonstrated that guggulsterone can be released from these biodegradable microspheres over 44 days. In addition, these drug-releasing microspheres were successfully incorporated within PSC-derived neural aggregates as a proof of concept. On-going work is aimed at evaluating the effectiveness of the guggulsterone-encapusulated microspheres in producing mature functional DNs from hiPSCs.

Bibliography

Agbay, A., Mohtaram, N. K., & Willerth, S. M. (2014). Controlled release of glial cell line-derived neurotrophic factor from poly(epsilon-caprolactone) microspheres. *Drug Deliv Transl Res, 4*(2), 159-170. doi: 10.1007/s13346-013-0189-0

Ahn, K. S., Sethi, G., Sung, B., Goel, A., Ralhan, R., & Aggarwal, B. B. (2008). Guggulsterone, a farnesoid X receptor antagonist, inhibits constitutive and inducible STAT3 activation through induction of a protein tyrosine phosphatase SHP-1. *Cancer Res, 68*(11), 4406-4415. doi: 10.1158/0008-5472.can-07-6696

Akhade, M. S., Agrawal, P. A., & Laddha, K. S. (2013). Development and Validation of RP-HPLC Method for Simultaneous Estimation of Picroside I, Plumbagin, and Z-guggulsterone in Tablet Formulation. *Indian J Pharm Sci, 75*(4), 476-482. doi: 10.4103/0250-474x.119835

Arenas, E., Denham, M., & Villaescusa, J. C. (2015). How to make a midbrain dopaminergic neuron. *Development, 142*(11), 1918-1936. doi: 10.1242/dev.097394

Atyabi, S. M., Sharifi, F., Irani, S., Zandi, M., Mivehchi, H., & Nagheh, Z. (2016). Cell Attachment and Viability Study of PCL Nano-fiber Modified by Cold Atmospheric Plasma. *Cell Biochem Biophys, 74*(2), 181-190. doi: 10.1007/s12013-015-0718-1

Basson, M. A., Echevarria, D., Ahn, C. P., Sudarov, A., Joyner, A. L., Mason, I. J., . . . Martin, G. R. (2008). Specific regions within the embryonic midbrain and cerebellum require different levels of FGF signaling during development. *Development, 135*(5), 889-898. doi: 10.1242/dev.011569

Beck, K. D., Valverde, J., Alexi, T., Poulsen, K., Moffat, B., Vandlen, R. A., . . . Hefti, F. (1995). Mesencephalic dopaminergic neurons protected by GDNF from axotomy-induced degeneration in the adult brain. *Nature, 373*(6512), 339-341. doi: 10.1038/373339a0

Beck, L. R., Pope, V. Z., Tice, T. R., & Gilley, R. M. (1985). Long-acting injectable microsphere formulation for the parenteral administration of levonorgestrel. *Adv Contracept, 1*(2), 119-129.

Becker, A. J., Mc, C. E., & Till, J. E. (1963). Cytological demonstration of the clonal nature of spleen colonies derived from transplanted mouse marrow cells. *Nature, 197*, 452-454.

Beitz, J. M. (2014). Parkinson's disease: a review. *Front Biosci (Schol Ed), 6*, 65-74.

Benowitz, L. I., & Yin, Y. (2007). Combinatorial treatments for promoting axon regeneration in the CNS: strategies for overcoming inhibitory signals and activating neurons' intrinsic growth state. *Dev Neurobiol, 67*(9), 1148-1165. doi: 10.1002/dneu.20515

Bieberich, E., & Wang, G. (2013). *Molecular Mechanisms Underlying Pluripotency*: InTech.

Blandini, F., Nappi, G., Tassorelli, C., & Martignoni, E. (2000). Functional changes of the basal ganglia circuitry in Parkinson's disease. *Prog Neurobiol, 62*(1), 63-88.

Bramfeldt, H., & Vermette, P. (2009). Enhanced smooth muscle cell adhesion and proliferation on protein-modified polycaprolactone-based copolymers. *J Biomed Mater Res A, 88*(2), 520-530. doi: 10.1002/jbm.a.31889

Bratt-Leal, A. M., Carpenedo, R. L., & McDevitt, T. C. (2009). Engineering the embryoid body microenvironment to direct embryonic stem cell differentiation. *Biotechnol Prog, 25*(1), 43-51. doi: 10.1002/btpr.139

Bratt-Leal, A. M., Carpenedo, R. L., Ungrin, M. D., Zandstra, P. W., & McDevitt, T. C. (2011). Incorporation of biomaterials in multicellular aggregates modulates pluripotent stem cell differentiation. *Biomaterials, 32*(1), 48-56. doi: 10.1016/j.biomaterials.2010.08.113

Bratt-Leal, A. M., Nguyen, A. H., Hammersmith, K. A., Singh, A., & McDevitt, T. C. (2013). A microparticle approach to morphogen delivery within pluripotent stem cell aggregates. *Biomaterials, 34*(30), 7227-7235. doi: 10.1016/j.biomaterials.2013.05.079

Brennan, J., Lu, C. C., Norris, D. P., Rodriguez, T. A., Beddington, R. S., & Robertson, E. J. (2001). Nodal signalling in the epiblast patterns the early mouse embryo. *Nature, 411*(6840), 965-969. doi: 10.1038/35082103

Briscoe, J. (2006). Agonizing hedgehog. *Nat Chem Biol, 2*(1), 10-11. doi: 10.1038/nchembio0106-10

Buettner, R., Mora, L. B., & Jove, R. (2002). Activated STAT signaling in human tumors provides novel molecular targets for therapeutic intervention. *Clin Cancer Res, 8*(4), 945-954.

Carpenedo, R. L., Bratt-Leal, A. M., Marklein, R. A., Seaman, S. A., Bowen, N. J., McDonald, J. F., & McDevitt, T. C. (2009). Homogeneous and organized differentiation within embryoid bodies induced by microsphere-mediated delivery of small molecules. *Biomaterials, 30*(13), 2507-2515. doi: 10.1016/j.biomaterials.2009.01.007

Carpenedo, R. L., Seaman, S. A., & McDevitt, T. C. (2010). Microsphere size effects on embryoid body incorporation and embryonic stem cell differentiation. *J Biomed Mater Res A, 94*(2), 466-475. doi: 10.1002/jbm.a.32710

Castelo-Branco, G., Rawal, N., & Arenas, E. (2004). GSK-3beta inhibition/beta-catenin stabilization in ventral midbrain precursors increases differentiation into dopamine neurons. *J Cell Sci, 117*(Pt 24), 5731-5737. doi: 10.1242/jcs.01505

Castelo-Branco, G., Wagner, J., Rodriguez, F. J., Kele, J., Sousa, K., Rawal, N., . . . Arenas, E. (2003). Differential regulation of midbrain dopaminergic neuron development by Wnt-1, Wnt-3a, and Wnt-5a. *Proc Natl Acad Sci U S A, 100*(22), 12747-12752. doi: 10.1073/pnas.1534900100

Chambers, S. M., Fasano, C. A., Papapetrou, E. P., Tomishima, M., Sadelain, M., & Studer, L. (2009). Highly efficient neural conversion of human ES and iPS cells by dual inhibition of SMAD signaling. *Nat Biotechnol, 27*(3), 275-280. doi: 10.1038/nbt.1529

Chen, G., Gulbranson, D. R., Hou, Z., Bolin, J. M., Ruotti, V., Probasco, M. D., . . . Thomson, J. A. (2011). Chemically defined conditions for human iPSC derivation and culture. *Nat Methods, 8*(5), 424-429. doi: 10.1038/nmeth.1593

Chen, K. G., Mallon, B. S., McKay, R. D., & Robey, P. G. (2014). Human pluripotent stem cell culture: considerations for maintenance, expansion, and therapeutics. *Cell Stem Cell, 14*(1), 13-26. doi: 10.1016/j.stem.2013.12.005

Chen, X., Vega, V. B., & Ng, H. H. (2008). Transcriptional regulatory networks in embryonic stem cells. *Cold Spring Harb Symp Quant Biol, 73*, 203-209. doi: 10.1101/sqb.2008.73.026

Chi, C. L., Martinez, S., Wurst, W., & Martin, G. R. (2003). The isthmic organizer signal FGF8 is required for cell survival in the prospective midbrain and cerebellum. *Development, 130*(12), 2633-2644.

Chinta, S. J., & Andersen, J. K. (2005). Dopaminergic neurons. *The International Journal of Biochemistry & Cell Biology, 37*(5), 942-946. doi: http://dx.doi.org/10.1016/j.biocel.2004.09.009

Chung, T. W., Wang, S. S., Wang, Y. Z., Hsieh, C. H., & Fu, E. (2009). Enhancing growth and proliferation of human gingival fibroblasts on chitosan grafted poly (epsilon-caprolactone) films is influenced by nano-roughness chitosan surfaces. *J Mater Sci Mater Med, 20*(1), 397-404. doi: 10.1007/s10856-008-3586-z

Coccoli, V., Luciani, A., Orsi, S., Guarino, V., Causa, F., & Netti, P. A. (2008). Engineering of poly(epsilon-caprolactone) microcarriers to modulate protein encapsulation capability and release kinetic. *J Mater Sci Mater Med, 19*(4), 1703-1711. doi: 10.1007/s10856-007-3253-9

Corson, L. B., Yamanaka, Y., Lai, K. M., & Rossant, J. (2003). Spatial and temporal patterns of ERK signaling during mouse embryogenesis. *Development, 130*(19), 4527-4537. doi: 10.1242/dev.00669

Costantini, L. C., & Isacson, O. (2000). Immunophilin ligands and GDNF enhance neurite branching or elongation from developing dopamine neurons in culture. *Exp Neurol, 164*(1), 60-70. doi: 10.1006/exnr.2000.7417

Crawford, T. Q., & Roelink, H. (2007). The notch response inhibitor DAPT enhances neuronal differentiation in embryonic stem cell-derived embryoid bodies independently of sonic hedgehog signaling. *Dev Dyn, 236*(3), 886-892. doi: 10.1002/dvdy.21083

Crossley, P. H., Martinez, S., & Martin, G. R. (1996). Midbrain development induced by FGF8 in the chick embryo. *Nature, 380*(6569), 66-68. doi: 10.1038/380066a0

Dauer, W., & Przedborski, S. (2003). Parkinson's disease: mechanisms and models. *Neuron, 39*(6), 889-909.

de Lau, L. M., & Breteler, M. M. (2006). Epidemiology of Parkinson's disease. *Lancet Neurol, 5*(6), 525-535. doi: 10.1016/s1474-4422(06)70471-9

Dutta, D., Salifu, M., Sirianni, R. W., & Stabenfeldt, S. E. (2015). Tailoring Sub-Micron PLGA Particle Release Profiles via Centrifugal Fractioning. *J Biomed Mater Res A*. doi: 10.1002/jbm.a.35608

El-Akabawy, G., Medina, L. M., Jeffries, A., Price, J., & Modo, M. (2011). Purmorphamine increases DARPP-32 differentiation in human striatal neural stem cells through the Hedgehog pathway. *Stem Cells Dev, 20*(11), 1873-1887. doi: 10.1089/scd.2010.0282

Evans, M. J., & Kaufman, M. H. (1981). Establishment in culture of pluripotential cells from mouse embryos. *Nature, 292*(5819), 154-156.

Fahn, S. (2015). The medical treatment of Parkinson disease from James Parkinson to George Cotzias. *Mov Disord, 30*(1), 4-18. doi: 10.1002/mds.26102

Fasano, C. A., Chambers, S. M., Lee, G., Tomishima, M. J., & Studer, L. (2010). Efficient derivation of functional floor plate tissue from human embryonic stem cells. *Cell Stem Cell, 6*(4), 336-347. doi: 10.1016/j.stem.2010.03.001

Ferreira, L., Squier, T., Park, H., Choe, H., Kohane, D. S., & Langer, R. (2008). Human Embryoid Bodies Containing Nano- and Microparticulate Delivery Vehicles. *Advanced Materials, 20*(12), 2285-2291. doi: 10.1002/adma.200702404

Friling, S., Andersson, E., Thompson, L. H., Jonsson, M. E., Hebsgaard, J. B., Nanou, E., . . . Ericson, J. (2009). Efficient production of mesencephalic dopamine neurons

by Lmx1a expression in embryonic stem cells. *Proc Natl Acad Sci U S A, 106*(18), 7613-7618. doi: 10.1073/pnas.0902396106

Gage, F. H., & Temple, S. (2013). Neural stem cells: generating and regenerating the brain. *Neuron, 80*(3), 588-601. doi: 10.1016/j.neuron.2013.10.037

Garcia-Ptacek, S., & Kramberger, M. G. (2016). Parkinson Disease and Dementia. *J Geriatr Psychiatry Neurol, 29*(5), 261-270. doi: 10.1177/0891988716654985

Giunchedi, P., Alpar, H. O., & Conte, U. (1998). PDLLA microspheres containing steroids: spray-drying, o/w and w/o/w emulsifications as preparation methods. *J Microencapsul, 15*(2), 185-195. doi: 10.3109/02652049809006848

Gomez, J. C., Edgar, J. M., Agbay, A. M., Bibault, E., Montgomery, A., Mohtaram, N. K., & Willerth, S. M. (2015). Incorporation of Retinoic Acid Releasing Microspheres into Pluripotent Stem Cell Aggregates for Inducing Neuronal Differentiation. [journal article]. *Cellular and Molecular Bioengineering, 8*(3), 307-319. doi: 10.1007/s12195-015-0401-z

Gonzalez, R., Garitaonandia, I., Abramihina, T., Wambua, G. K., Ostrowska, A., Brock, M., . . . Semechkin, R. A. (2013). Deriving dopaminergic neurons for clinical use. A practical approach. *Sci Rep, 3*, 1463. doi: 10.1038/srep01463

Gorman, A. M. (2008). Neuronal cell death in neurodegenerative diseases: recurring themes around protein handling. *J Cell Mol Med, 12*(6a), 2263-2280. doi: 10.1111/j.1582-4934.2008.00402.x

Hegarty, S. V., Sullivan, A. M., & O'Keeffe, G. W. (2013). Midbrain dopaminergic neurons: a review of the molecular circuitry that regulates their development. *Dev Biol, 379*(2), 123-138. doi: 10.1016/j.ydbio.2013.04.014

Hely, M. A., Morris, J. G., Traficante, R., Reid, W. G., O'Sullivan, D. J., & Williamson, P. M. (1999). The sydney multicentre study of Parkinson's disease: progression and mortality at 10 years. *J Neurol Neurosurg Psychiatry, 67*(3), 300-307.

Hong, S., & Song, M. R. (2014). STAT3 but not STAT1 is required for astrocyte differentiation. *PLoS One, 9*(1), e86851. doi: 10.1371/journal.pone.0086851

Huang, C., Wang, J., Lu, X., Hu, W., Wu, F., Jiang, B., . . . Zhang, W. (2016). Z-guggulsterone negatively controls microglia-mediated neuroinflammation via blocking IkappaB-alpha-NF-kappaB signals. *Neurosci Lett, 619*, 34-42. doi: 10.1016/j.neulet.2016.02.021

Jaber, M., Robinson, S. W., Missale, C., & Caron, M. G. (1996). Dopamine receptors and brain function. *Neuropharmacology, 35*(11), 1503-1519. doi: https://doi.org/10.1016/S0028-3908(96)00100-1

James, D., Levine, A. J., Besser, D., & Hemmati-Brivanlou, A. (2005). TGFbeta/activin/nodal signaling is necessary for the maintenance of pluripotency in human embryonic stem cells. *Development, 132*(6), 1273-1282. doi: 10.1242/dev.01706

Jankovic, J., & Aguilar, L. G. (2008). Current approaches to the treatment of Parkinson's disease. *Neuropsychiatr Dis Treat, 4*(4), 743-757.

Jeong, Y. I., Song, J. G., Kang, S. S., Ryu, H. H., Lee, Y. H., Choi, C., . . . Jung, S. (2003). Preparation of poly(DL-lactide-co-glycolide) microspheres encapsulating all-trans retinoic acid. *Int J Pharm, 259*(1-2), 79-91.

Joyner, A. L., Liu, A., & Millet, S. (2000). Otx2, Gbx2 and Fgf8 interact to position and maintain a mid-hindbrain organizer. *Curr Opin Cell Biol, 12*(6), 736-741.

Kalia, L. V., & Lang, A. E. (2016). Parkinson disease in 2015: Evolving basic, pathological and clinical concepts in PD. [Year in Review]. *Nat Rev Neurol, 12*(2), 65-66. doi: 10.1038/nrneurol.2015.249

Kim, K., Doi, A., Wen, B., Ng, K., Zhao, R., Cahan, P., . . . Daley, G. Q. (2010). Epigenetic memory in induced pluripotent stem cells. *Nature, 467*(7313), 285-290. doi: 10.1038/nature09342

Kirkeby, A., Grealish, S., Wolf, D. A., Nelander, J., Wood, J., Lundblad, M., . . . Parmar, M. (2012). Generation of regionally specified neural progenitors and functional neurons from human embryonic stem cells under defined conditions. *Cell Rep, 1*(6), 703-714. doi: 10.1016/j.celrep.2012.04.009

Kriks, S., Shim, J. W., Piao, J., Ganat, Y. M., Wakeman, D. R., Xie, Z., . . . Studer, L. (2011). Dopamine neurons derived from human ES cells efficiently engraft in animal models of Parkinson's disease. *Nature, 480*(7378), 547-551. doi: 10.1038/nature10648

Lake, J., Rathjen, J., Remiszewski, J., & Rathjen, P. D. (2000). Reversible programming of pluripotent cell differentiation. *J Cell Sci, 113 (Pt 3)*, 555-566.

Lee, S. H., Lumelsky, N., Studer, L., Auerbach, J. M., & McKay, R. D. (2000). Efficient generation of midbrain and hindbrain neurons from mouse embryonic stem cells. *Nat Biotechnol, 18*(6), 675-679. doi: 10.1038/76536

Lim, J. J., Hammoudi, T. M., Bratt-Leal, A. M., Hamilton, S. K., Kepple, K. L., Bloodworth, N. C., . . . Temenoff, J. S. (2011). Development of nano- and microscale chondroitin sulfate particles for controlled growth factor delivery. *Acta Biomater, 7*(3), 986-995. doi: 10.1016/j.actbio.2010.10.009

Martin, G. R. (1981). Isolation of a pluripotent cell line from early mouse embryos cultured in medium conditioned by teratocarcinoma stem cells. *Proc Natl Acad Sci U S A, 78*(12), 7634-7638.

Martinez, S., Crossley, P. H., Cobos, I., Rubenstein, J. L., & Martin, G. R. (1999). FGF8 induces formation of an ectopic isthmic organizer and isthmocerebellar development via a repressive effect on Otx2 expression. *Development, 126*(6), 1189-1200.

Mena, M. A., Casarejos, M. J., Bonin, A., Ramos, J. A., & Garcia Yebenes, J. (1995). Effects of dibutyryl cyclic AMP and retinoic acid on the differentiation of dopamine neurons: prevention of cell death by dibutyryl cyclic AMP. *J Neurochem, 65*(6), 2612-2620.

Miyasaki, J. M. (2016). Treatment of Advanced Parkinson Disease and Related Disorders. *Continuum (Minneap Minn), 22*(4 Movement Disorders), 1104-1116. doi: 10.1212/con.0000000000000347

Murry, C. E., & Keller, G. (2008). Differentiation of embryonic stem cells to clinically relevant populations: lessons from embryonic development. *Cell, 132*(4), 661-680. doi: 10.1016/j.cell.2008.02.008

Niederreither, K., Vermot, J., Schuhbaur, B., Chambon, P., & Dolle, P. (2000). Retinoic acid synthesis and hindbrain patterning in the mouse embryo. *Development, 127*(1), 75-85.

Niwa, H. (2007). How is pluripotency determined and maintained? *Development, 134*(4), 635-646. doi: 10.1242/dev.02787

Patthey, C., & Gunhaga, L. (2014). Signaling pathways regulating ectodermal cell fate choices. *Exp Cell Res, 321*(1), 11-16. doi: 10.1016/j.yexcr.2013.08.002

Perrier, A. L., Tabar, V., Barberi, T., Rubio, M. E., Bruses, J., Topf, N., . . . Studer, L. (2004). Derivation of midbrain dopamine neurons from human embryonic stem cells. *Proc Natl Acad Sci U S A, 101*(34), 12543-12548. doi: 10.1073/pnas.0404700101

Placzek, M., & Briscoe, J. (2005). The floor plate: multiple cells, multiple signals. *Nat Rev Neurosci, 6*(3), 230-240. doi: 10.1038/nrn1628

Postuma, R. B., Berg, D., Stern, M., Poewe, W., Olanow, C. W., Oertel, W., . . . Deuschl, G. (2015). MDS clinical diagnostic criteria for Parkinson's disease. *Mov Disord, 30*(12), 1591-1601. doi: 10.1002/mds.26424

Qutachi, O., Shakesheff, K. M., & Buttery, L. D. (2013). Delivery of definable number of drug or growth factor loaded poly(DL-lactic acid-co-glycolic acid) microparticles within human embryonic stem cell derived aggregates. *J Control Release, 168*(1), 18-27. doi: 10.1016/j.jconrel.2013.02.029

Recek, N., Resnik, M., Motaln, H., Lah-Turn, #x161, ek, T., . . . , M. (2016). Cell Adhesion on Polycaprolactone Modified by Plasma Treatment. *International Journal of Polymer Science, 2016*, 9. doi: 10.1155/2016/7354396

Reynolds, B. A., & Weiss, S. (1992). Generation of neurons and astrocytes from isolated cells of the adult mammalian central nervous system. *Science, 255*(5052), 1707-1710.

Robinson, M., Yau, S.-y., Sun, L., Gabers, N., Bibault, E., Christie, B. R., & Willerth, S. M. (2015). Optimizing Differentiation Protocols for Producing Dopaminergic Neurons from Human Induced Pluripotent Stem Cells for Tissue Engineering Applications. *Biomarker Insights*(Supplementary Video 20064), 61-70. doi: 10.4137/bmi.s20064

Rodda, D. J., Chew, J. L., Lim, L. H., Loh, Y. H., Wang, B., Ng, H. H., & Robson, P. (2005). Transcriptional regulation of nanog by OCT4 and SOX2. *J Biol Chem, 280*(26), 24731-24737. doi: 10.1074/jbc.M502573200

Roussa, E., von Bohlen und Halbach, O., & Krieglstein, K. (2009). TGF-beta in dopamine neuron development, maintenance and neuroprotection. *Adv Exp Med Biol, 651*, 81-90.

Sachlos, E., & Auguste, D. T. (2008). Embryoid body morphology influences diffusive transport of inductive biochemicals: a strategy for stem cell differentiation. *Biomaterials, 29*(34), 4471-4480. doi: 10.1016/j.biomaterials.2008.08.012

Sato, N., Sanjuan, I. M., Heke, M., Uchida, M., Naef, F., & Brivanlou, A. H. (2003). Molecular signature of human embryonic stem cells and its comparison with the mouse. *Dev Biol, 260*(2), 404-413.

Shishodia, S., Azu, N., Rosenzweig, J. A., & Jackson, D. A. (2016). Guggulsterone for Chemoprevention of Cancer. *Curr Pharm Des, 22*(3), 294-306.

Shutova, M. V., Surdina, A. V., Ischenko, D. S., Naumov, V. A., Bogomazova, A. N., Vassina, E. M., . . . Kiselev, S. L. (2016). An integrative analysis of reprogramming in human isogenic system identified a clone selection criterion. *Cell Cycle, 15*(7), 986-997. doi: 10.1080/15384101.2016.1152425

Sinha, V. R., Bansal, K., Kaushik, R., Kumria, R., & Trehan, A. (2004). Poly-epsilon-caprolactone microspheres and nanospheres: an overview. [Review]. *International Journal of Pharmaceutics, 278*(1), 1-23. doi: 10.1016/j.ijpharm.2004.01.044

Stoker, T. B., & Barker, R. A. (2016). Cell therapies for Parkinson's disease: how far have we come? *Regen Med, 11*(8), 777-786. doi: 10.2217/rme-2016-0102

Takahashi, K., Tanabe, K., Ohnuki, M., Narita, M., Ichisaka, T., Tomoda, K., & Yamanaka, S. (2007). Induction of pluripotent stem cells from adult human fibroblasts by defined factors. *Cell, 131*(5), 861-872. doi: 10.1016/j.cell.2007.11.019

Takahashi, K., & Yamanaka, S. (2006). Induction of pluripotent stem cells from mouse embryonic and adult fibroblast cultures by defined factors. *Cell, 126*(4), 663-676. doi: 10.1016/j.cell.2006.07.024

Tang, M., Villaescusa, J. C., Luo, S. X., Guitarte, C., Lei, S., Miyamoto, Y., . . . Huang, E. J. (2010). Interactions of Wnt/beta-catenin signaling and sonic hedgehog regulate the neurogenesis of ventral midbrain dopamine neurons. *J Neurosci, 30*(27), 9280-9291. doi: 10.1523/jneurosci.0860-10.2010

Thomson, J. A., Itskovitz-Eldor, J., Shapiro, S. S., Waknitz, M. A., Swiergiel, J. J., Marshall, V. S., & Jones, J. M. (1998). Embryonic stem cell lines derived from human blastocysts. *Science, 282*(5391), 1145-1147.

Vallier, L., Alexander, M., & Pedersen, R. A. (2005). Activin/Nodal and FGF pathways cooperate to maintain pluripotency of human embryonic stem cells. *J Cell Sci, 118*(Pt 19), 4495-4509. doi: 10.1242/jcs.02553

van den Brink, S. C., Baillie-Johnson, P., Balayo, T., Hadjantonakis, A. K., Nowotschin, S., Turner, D. A., & Martinez Arias, A. (2014). Symmetry breaking, germ layer specification and axial organisation in aggregates of mouse embryonic stem cells. *Development, 141*(22), 4231-4242. doi: 10.1242/dev.113001

Van Den Eeden, S. K., Tanner, C. M., Bernstein, A. L., Fross, R. D., Leimpeter, A., Bloch, D. A., & Nelson, L. M. (2003). Incidence of Parkinson's disease: variation by age, gender, and race/ethnicity. *Am J Epidemiol, 157*(11), 1015-1022.

Van Winkle, A. P., Gates, I. D., & Kallos, M. S. (2012). Mass transfer limitations in embryoid bodies during human embryonic stem cell differentiation. *Cells Tissues Organs, 196*(1), 34-47. doi: 10.1159/000330691

Varde, N. K., & Pack, D. W. (2004). Microspheres for controlled release drug delivery. *Expert Opin Biol Ther, 4*(1), 35-51. doi: 10.1517/14712598.4.1.35

Wang, Y., Yu, X., Baker, C., Murphy, W. L., & McDevitt, T. C. (2016). Mineral particles modulate osteo-chondrogenic differentiation of embryonic stem cell aggregates. *Acta Biomater, 29*, 42-51. doi: 10.1016/j.actbio.2015.10.039

Weerkamp, N. J., Tissingh, G., Poels, P. J., Zuidema, S. U., Munneke, M., Koopmans, R. T., & Bloem, B. R. (2013). Nonmotor symptoms in nursing home residents with Parkinson's disease: prevalence and effect on quality of life. *J Am Geriatr Soc, 61*(10), 1714-1721. doi: 10.1111/jgs.12458

Wen, S., Li, H., & Liu, J. (2009). Dynamic signaling for neural stem cell fate determination. *Cell Adh Migr, 3*(1), 107-117.

Wilmut, I., Schnieke, A. E., McWhir, J., Kind, A. J., & Campbell, K. H. (1997). Viable offspring derived from fetal and adult mammalian cells. *Nature, 385*(6619), 810-813. doi: 10.1038/385810a0

Wilson, P. G., & Stice, S. S. (2006). Development and differentiation of neural rosettes derived from human embryonic stem cells. *Stem Cell Rev, 2*(1), 67-77. doi: 10.1007/s12015-006-0011-1

Woodruff, M. A., & Hutmacher, D. W. (2010). The return of a forgotten polymer—Polycaprolactone in the 21st century. *Progress in Polymer Science, 35*(10), 1217-1256. doi: http://dx.doi.org/10.1016/j.progpolymsci.2010.04.002

Xiao, L., Yuan, X., & Sharkis, S. J. (2006). Activin A maintains self-renewal and regulates fibroblast growth factor, Wnt, and bone morphogenic protein pathways in human embryonic stem cells. *Stem Cells, 24*(6), 1476-1486. doi: 10.1634/stemcells.2005-0299

Xu, R. H., Peck, R. M., Li, D. S., Feng, X., Ludwig, T., & Thomson, J. A. (2005). Basic FGF and suppression of BMP signaling sustain undifferentiated proliferation of human ES cells. *Nat Methods, 2*(3), 185-190. doi: 10.1038/nmeth744

Yamada, T., & Sugimoto, K. (2016). Guggulsterone and Its Role in Chronic Diseases. *Adv Exp Med Biol, 929*, 329-361. doi: 10.1007/978-3-319-41342-6_15

Yan, J., Studer, L., & McKay, R. D. (2001). Ascorbic acid increases the yield of dopaminergic neurons derived from basic fibroblast growth factor expanded mesencephalic precursors. *J Neurochem, 76*(1), 307-311.

Yan, Y., Yang, D., Zarnowska, E. D., Du, Z., Werbel, B., Valliere, C., . . . Zhang, S. C. (2005). Directed differentiation of dopaminergic neuronal subtypes from human embryonic stem cells. *Stem Cells, 23*(6), 781-790. doi: 10.1634/stemcells.2004-0365

Yang, Y. Y., Chung, T. S., & Ng, N. P. (2001). Morphology, drug distribution, and in vitro release profiles of biodegradable polymeric microspheres containing protein fabricated by double-emulsion solvent extraction/evaporation method. *Biomaterials, 22*(3), 231-241.

Ye, W., Shimamura, K., Rubenstein, J. L., Hynes, M. A., & Rosenthal, A. (1998). FGF and Shh signals control dopaminergic and serotonergic cell fate in the anterior neural plate. *Cell, 93*(5), 755-766.

Yildirim, E. D., Besunder, R., Pappas, D., Allen, F., Guceri, S., & Sun, W. (2010). Accelerated differentiation of osteoblast cells on polycaprolactone scaffolds driven by a combined effect of protein coating and plasma modification. *Biofabrication, 2*(1), 014109. doi: 10.1088/1758-5082/2/1/014109

Zhang, S. C., Wernig, M., Duncan, I. D., Brustle, O., & Thomson, J. A. (2001). In vitro differentiation of transplantable neural precursors from human embryonic stem cells. *Nat Biotechnol, 19*(12), 1129-1133. doi: 10.1038/nbt1201-1129

Zhao, C. X. (2013). Multiphase flow microfluidics for the production of single or multiple emulsions for drug delivery. *Adv Drug Deliv Rev, 65*(11-12), 1420-1446. doi: 10.1016/j.addr.2013.05.009